

Solitary water wave interactions

W. Craig*

Department of Mathematics, McMaster University, Hamilton, ON L8S 4K1, Canada

P. Guyenne

Department of Mathematics, University of Delaware, Newark, DE 19716-2553, USA

J. Hammack and D. Henderson

Department of Mathematics, Pennsylvania State University, University Park, PA 16802, USA

C. Sulem

Department of Mathematics, University of Toronto, Toronto, ON M5S 2E4, Canada

(Dated: December 20, 2005)

This article concerns the pairwise nonlinear interaction of solitary waves in the free surface of a body of water lying over a horizontal bottom. Unlike solitary waves in many completely integrable model systems, solitary waves for the full Euler equations do not collide elastically; after interactions there is a nonzero residual wave which trails the post-collision solitary waves. In this report on new numerical and experimental studies of such solitary wave interactions, we verify that this is the case, both in head-on collisions (the counter-propagating case) and overtaking collisions (the co-propagating case), quantifying the degree to which interactions are inelastic. In the situation in which two identical solitary waves undergo a head-on collision, we compare the asymptotic predictions of Su and Mirie [6] and Byatt-Smith [23], the wavetank experiments of Maxworthy [5], and the numerical results of Cooker, Weidman and Bale [4] with independent numerical simulations, in which we quantify the phase change, the run-up, and the form of the residual wave and its Fourier signature in both small and large amplitude interactions. This updates the prior numerical observations of inelastic interactions in Fenton and Rienecker [3]. In the case of two non-identical solitary waves, our precision wavetank experiments are compared with numerical simulations, again observing the run up, phase lag, and the generation of a residual from the interaction. Considering overtaking solitary wave interactions, we compare our experimental observations, numerical simulations, and the asymptotic predictions of Zou and Su [14], and again we quantify the inelastic residual after collisions in the simulations. Geometrically, our numerical simulations of overtaking interactions fit into the three categories of KdV two-soliton solutions defined in Lax [16], with however a modification in the parameter regime. In all cases we have considered, collisions are seen to be inelastic, although the degree to which interactions depart from elastic is very small. Finally, we give several theoretical results: (1) a relationship between the change in amplitude of solitary waves due to a pairwise collision and the energy carried away from the interaction by the residual component, and (2) a rigorous estimate of the size of the residual component of pairwise solitary wave collisions. This estimate is consistent with the analytic results of Schneider and Wayne [20], Wright [22] and Bona, Colin and Lannes [21]. However in the light of our numerical data, both (1) and (2) indicate a need to re-evaluate the asymptotic results in [6, 14].

PACS numbers: Valid PACS appear here

I. INTRODUCTION

Solitary waves for the Euler equations have been a topic of interest since the time of Stokes [1]. In a small amplitude long wave perturbation regime they are well described by single soliton solutions of the Korteweg – deVries equation (KdV), and it is a famous result that the multiple soliton solution of the KdV equation exhibits elastic collisions. The question is as to what extent interactions between solitary waves for Euler's equations fail to do so. We report on new numerical, experimen-

tal and analytical results on this point, concerning both co-propagating and counter-propagating cases in a range of small through large amplitude solitary waves. In all cases we quantify the degree to which interactions are inelastic, and one of our principal results is the study of the existence and the characteristics of the residual wave resulting from these interactions. However it is remarkable to us how small the residual is from a collision of even very large solitary waves.

In the case of a collision of two counter-propagating solitary waves, prior numerical studies of solutions of the full Euler equations have been published by Chan and Street [2], Fenton and Rienecker [3] and Cooker, Weidman and Bale [4]. For the case of equal amplitudes, we provide independent verification of the numerical results of the latter reference, and we recover their accurate ob-

*Electronic address: craig@math.mcmaster.ca

servations of wave interactions with regard to the *run-up* (or superlinear amplitude increase) on the axis of symmetry of the interaction, the *phase lag* due to collisions, and the *wall residence time* (or period of concurrence of the wave crests). This information is compared with the experimental observations of Maxworthy [5], and with the asymptotic predictions for the run-up and the phase lag in Su and Mirie [6] (related to the prior discussions of these quantities in Byatt-Smith [7] and Oikawa and Yajima [8]). In addition we report on the change in amplitude (and subsequent change in velocity) of the solitary wave components due to the collision, and we provide a description of the residual component, the *residual* of the solution after the interaction in terms of its Fourier spectrum. We find that after a sufficient time interval, the post-collision solitary waves separate from each other *and* from the support of the trailing residual wave; this suggests that within the amplitude ranges we considered, solitary waves are stable to disturbances in the form of pairwise collisions.

The numerical method to reproduce precise solitary wave profiles of specified amplitude is based on a modification of the method of Tanaka [9]. For well resolved simulations of time evolution we use a surface spectral method of Craig and Sulem [10], which is sufficiently accurate to resolve detailed features in solutions which are up to four orders of magnitude smaller than the amplitudes of the incident solitary waves. We wish to distinguish our work on Euler's equations from numerical studies of counter-propagating solitary waves for model problems, which have appeared in Mirie and Su [11] and Bona and Chen [12], among others; these give qualitative agreement with the above results without quantifying the precise details of the residual.

In the case of two counter-propagating solitary waves of different amplitude, we report on a direct comparison between our experimental observations of solitary wave interactions in the wave channel at Penn State University and numerical simulations of asymmetric solitary wave interactions using the above methods. We find that our simulations of the full Euler equations do well at predicting the measurements of the free surface from the wave channel experiments. Further numerical observations are given, focusing on the run-up and phase-lag (noting that a period of crest concurrence is not well defined in this context), and the generation of a residual resulting from the collision.

In the case of co-propagating (or overtaking) solitary wave interactions, we compare the results of our wave channel experiments with numerical simulations, finding that the numerical solutions are substantially more accurate in predicting the details of the interaction than the KdV equation (see however Hammack and Segur [13]). Our further numerical studies again show that there is always a residual after the interaction, a conclusion which is qualitatively consistent with the asymptotic predictions of Zou and Su [14]. This updates the findings of Fenton and Rienecker [3], who found no residual to

within the order of accuracy of their numerical scheme. The residual, as well as the changes in amplitudes and velocities of the solitary waves involved, are in fact very small in magnitude. Similar interactions of this general form are described by Bona, Pritchard and Scott [15] and Mirie and Su [11] in solutions of long-wave model equations. Quantitatively, the changes in amplitude and velocity are very different than for counter-propagating collisions; in the co-propagating case the larger overtaking wave gains amplitude while the smaller loses amplitude from the interaction, and the amplitude of the residual is approximately an order of magnitude smaller than in the counter-propagating case. In every case, the maximum amplitude of the solution at any time during the interaction is strictly less than the maximum amplitude of the largest individual solitary wave (the overtaking one). Focusing on the details of the interaction, we compare our experiments and the numerical solutions to the three regimes of KdV two-soliton interactions described by Lax [16], finding that, in a similar manner, solitary wave interactions maintain two distinct crests in a regime (a), fuse to form one central crest during the collision in a regime (c), and exhibit a regime (b) of intermediate type. While the character of the interaction is nearly identical, the solitary wave amplitudes at which the transitions occur between regimes are somewhat different than the KdV setting, a fact which has been previously noted in Fenton and Rienecker [3]. Our experimental results focus on the category (b), presenting unambiguous observations of this case (see Weidman and Maxworthy [17] for other experimental observations of this case and cases (a) and (c)). A discussion of the behavior of co-propagating interactions of solitary waves to a model problem, and a comparison with the Lax categories, are given in Wu [18].

Using the fact that the total mass, momentum and energy of free surface water waves are conserved, and the fact that solitary waves occur in a one parameter family, we derive two results. The first is a relationship between the change of amplitude of solitary waves due to a collision and the energy carried by the residual. Secondly, we prove a rigorous estimate giving an upper bound on the energy of the residual of a solitary wave interaction. The latter is based on three hypotheses, all of which are clearly consistent with our numerical and experimental observations, but none having yet an unimpeachable verification. The proof of this result is more straightforward than the results for general initial data given in Craig [19], and Schneider and Wayne [20], although it is a less accurate result. For more precise estimates we cite Bona, Colin and Lannes [21] and Wright [22], the latter giving the currently best rigorous result on the higher order correction terms. The data from our numerical simulations agree with these theoretical results, and indicate that the estimate of upper bounds scales with the correct order as the amplitude of the incoming solitary waves tends to zero. However our numerical data also show a discrepancy with the order predicted by the asymptotic calculations of Su and

Mirie [6] and Byatt-Smith [23].

The paper is organized as follows. In Sec. II we review the mathematical statement of the problem of water waves, and we reformulate the resulting evolution equations as a Hamiltonian system in terms of surface variables, following Zakharov [24], expressing the Hamiltonian in terms of the Dirichlet – Neumann operator as in Craig and Sulem [10]. We additionally describe our numerical methods based on this formulation, and we give a description of the experimental laboratory setup. In Sec. III we describe our results for symmetric counter-propagating solitary wave interactions, and in Sec. IV we study asymmetric cases, including comparisons of numerical computations with laboratory experiments. In Sec. V we give our experimental and numerical results for co-propagating solitary wave interactions. Section VI gives our straightforward and rigorous analysis of the energy loss and amplitude variation of solitary waves undergoing such collisions. A description of our modifications of Tanaka’s method (1986) of highly accurate approximations of solitary wave profiles is given in the appendix.

II. MATHEMATICAL FORMULATION

A. Governing equations

We consider the motion of a free surface of a two-dimensional fluid in a horizontal channel under the influence of gravity. The mean water level is located at $y = 0$ with y the vertical upward direction. The fluid is assumed to be incompressible, inviscid and irrotational, so that the velocity potential satisfies

$$\Delta\varphi = 0, \quad (1)$$

in the fluid region bounded by a uniform bottom $\{y = -h\}$ and the free surface $\{y = \eta(x, t)\}$, with the boundary conditions

$$\varphi_y = 0 \quad \text{on} \quad y = -h, \quad (2)$$

and

$$\left. \begin{aligned} \varphi_t + \frac{1}{2}(\nabla\varphi)^2 + g\eta &= 0 \\ \eta_t + \eta_x \varphi_x - \varphi_y &= 0 \end{aligned} \right\} \quad \text{on} \quad y = \eta(x, t), \quad (3)$$

where g is the acceleration due to gravity and subscripts denote differentiation with respect to the corresponding variables.

Following Zakharov [24] and Craig and Sulem [10], let $\xi(x, t) = \varphi(x, \eta(x, t), t)$ be the value of the velocity potential on the free surface, and define the Dirichlet–Neumann operator

$$G(\eta)\xi = \sqrt{1 + \eta_x^2} \varphi_n \Big|_{y=\eta}, \quad (4)$$

which maps Dirichlet data to Neumann data on the free surface, with n the unit exterior normal to the boundary.

This operator is linear in ξ but it is nonlinear with explicit nonlocal behaviour in η which determines the fluid domain. In terms of the surface quantities η and ξ , the boundary conditions (3) can be rewritten as

$$\begin{aligned} \eta_t &= G(\eta)\xi, \\ \xi_t &= \frac{-1}{2(1 + \eta_x^2)} [\xi_x^2 - (G(\eta)\xi)^2 - 2\eta_x \xi_x G(\eta)\xi] - g\eta \end{aligned} \quad (5)$$

These equations are Hamilton’s canonical equations in Zakharov’s formulation of the water wave problem as a Hamiltonian system, with Hamiltonian

$$H(\eta, \xi) = \frac{1}{2} \int_{-\infty}^{\infty} \xi G(\eta)\xi + g\eta^2 dx, \quad (7)$$

and the equations of evolution (5)(6) are in the form

$$\partial_t \begin{pmatrix} \eta \\ \xi \end{pmatrix} = \begin{pmatrix} 0 & 1 \\ -1 & 0 \end{pmatrix} \begin{pmatrix} \delta_\eta H \\ \delta_\xi H \end{pmatrix}. \quad (8)$$

The time evolution of (8) conserves a number of physical quantities, including the *added mass*

$$M(\eta) = \int_{-\infty}^{\infty} \eta(x, t) dx \quad (9)$$

and the momentum, or *impulse*

$$I(\eta, \xi) = \int_{-\infty}^{\infty} \eta(x, t) \partial_x \xi(x, t) dx. \quad (10)$$

This is verified by the following identities

$$\{M, H\} = 0 \quad , \quad \{I, H\} = 0, \quad (11)$$

where the *Poisson bracket* between two functionals F and H is given by

$$\{F, H\} = \int \delta_\eta F \delta_\xi H - \delta_\xi F \delta_\eta H dx. \quad (12)$$

Furthermore, the *center of mass* of a solution, given by

$$C(\eta) = \int_{-\infty}^{\infty} x\eta(x, t) dx \quad (13)$$

is a linear function of time. This is because its time derivative is a constant of motion;

$$\begin{aligned} \frac{d}{dt} C &= \int_{-\infty}^{\infty} x \partial_t \eta(x, t) dx \\ &= \int_{-\infty}^{\infty} x G(\eta)\xi dx = \int_{-\infty}^{\infty} \xi G(\eta)x dx \\ &= \int_{-\infty}^{\infty} \xi(-\partial_x \eta) dx = I(\eta, \xi). \end{aligned} \quad (14)$$

Equation (5) has been used in deducing the second line above, and expressions (3) and (4) in the third line.

Coifman and Meyer [25] showed that the Dirichlet–Neumann operator depends analytically on $\eta \in \text{Lip}(\mathbb{R})$, and therefore G can be written in terms of a convergent Taylor expansion

$$G(\eta) = \sum_{j=0}^{\infty} G_j(\eta), \quad (15)$$

where the Taylor polynomials G_j are homogeneous of degree j in η . Craig and Sulem [10] then showed that explicit expressions for G_j can be obtained using a recursion formula. The first three terms are given by

$$\begin{aligned} G_0 &= D \tanh(hD), \\ G_1 &= D\eta D - G_0\eta G_0, \\ G_2 &= \frac{1}{2} (G_0 D \eta^2 D - D^2 \eta^2 G_0 - 2G_0 \eta G_1), \end{aligned} \quad (16)$$

where $D = -i\partial_x$ and G_0 represent Fourier multiplier operators.

This formulation of the problem of water waves is convenient for the solitary wave interaction problem studied in this paper, as well as in a number of other settings. These include studies of long-wave asymptotics for waves over a rough bottom [26], waves in sharp interfaces between immiscible fluids [27], and numerical studies of the propagation of nonlinear water waves in a fluid domain with variable bathymetry [28].

B. Initial conditions

Initial conditions for the evolution equations (5)(6) are given by two well separated solitary waves, which are chosen to collide and then separate again in positive time, remaining within the experimental or computational domain. For the numerical simulations, data are taken to be solitary wave solutions $(\eta_S(x, t), \xi_S(x, t))$ on the classical bifurcation branch of solutions [29], [30], [9]. We have taken the bifurcation parameter to be $S \in [0, S_{max}]$ corresponding to amplitude $S = \|\eta_S(x)\|_{L^\infty}$. There are two basic cases; in the first, the velocities of the two waves have opposite signs (counter-propagating case), and their evolution will entail a collision in finite time and the subsequent separation of two modified solitary waves, leaving a small residual between them. The second case is of two solitary waves with velocities of the same sign (co-propagating case), the trailing wave being larger amplitude, which in time will ultimately overtake and interact with the leading wave. After the interaction there are again two separating, slightly modified solitary waves, and again a small residual, which in this case trails behind both. Initial data for the numerical simulations are approximations of the idealized situation in which the actual solution $(\eta_S(x, t), \xi_S(x, t))$ is asymptotic as $t \rightarrow -\infty$ to two infinitely separated solitary waves

$$\lim_{t \rightarrow -\infty} (\eta(x, t) - (\eta_{S_1}(x - c_1 t - a_1) + \eta_{S_2}(x - c_2 t - a_2))) = 0. \quad (17)$$

After the interaction, the solution $(\eta_S(x, t), \xi_S(x, t))$ will resume the form of two separating solitary wave profiles, with modified amplitudes $(S_1, S_2) \rightarrow (S_1^+, S_2^+)$ and phases $(a_1, a_2) \rightarrow (a_1^+, a_2^+)$, but with additionally a residual $(\eta_R(x, t), \xi_R(x, t))$ such that for large t ,

$$\begin{aligned} \eta(x, t) &= \eta_{S_1^+}(x - c_1^+ t - a_1^+) + \eta_{S_2^+}(x - c_2^+ t - a_2^+) \\ &\quad + \eta_R(x, t). \end{aligned} \quad (18)$$

A principal goal of this work is to study the details of solitary wave interactions, which include the scattering map $(S_1, S_2) \rightarrow (S_1^+, S_2^+)$, $(a_1, a_2) \rightarrow (a_1^+, a_2^+)$, as well as the amplitude and the character of the residual $(\eta_R(x, t), \xi_R(x, t))$ resulting from the collision.

C. Numerical methods

Numerical simulations of highly accurate solitary waves have a long history. We generate the solitary wave profiles for our initial data using a collocation method developed for the purpose; it is a version of the approach developed in Tanaka [9]. Fig. 1 is a plot of several solitary wave profiles $\eta_S(x)$ for different amplitudes S . Fig. 2 is a plot of the classical bifurcation branch of solitary wave profiles computed by the method, and Fig. 3 is a plot of the impulse as a function of mass for these solutions. The (slight) convexity of this graph over the majority of its range plays a rôle in the error analysis in Sec. VI. A description of the method and our modifications appears in the appendix.

The numerical methods used to solve the evolution equations (5) and (6) are similar to those proposed by Craig and Sulem [10]. We assume periodic boundary conditions in the x -direction and use a pseudospectral method for the space discretization of the problem. This is a natural choice for the computation of G since each term in (15) consists of concatenations of Fourier multipliers with powers of η . The Dirichlet–Neumann operator is approximated by a finite number of terms, i.e.

$$G(\eta) \simeq \sum_{j=0}^J G_j(\eta). \quad (19)$$

In practice, it is not necessary to use large values of J due to the fast convergence of the series expansion for G . Both the surface elevation η and velocity potential ξ are expanded in truncated Fourier series with the same number of modes. Applications of Fourier multipliers are performed in spectral space, while nonlinear products are calculated in physical space at a discrete set of N equally spaced points. Our numerical code has been developed from a set of routines for surface spectral methods by Nicholls [31]. All operations are performed using the FFTW routines by Frigo and Johnson [32]. For perturbations up to order J , the number of operations required is therefore $\mathcal{O}(J^2 N \ln N)$ per time step.

Time integration is performed in Fourier space. The linear terms in (5) and (6) are solved exactly by an integrating factor technique. The nonlinear terms are integrated using a fourth-order Adams–Bashford/Moulton predictor-corrector scheme with constant time step [33]. To initiate this scheme, the solution required at the first three time steps is provided by a fourth-order Runge–Kutta method. In the computations (especially of steep waves), it was observed that spurious oscillations can develop in the wave profile after some time of integration, due to onset of an instability related to the growth of numerical errors at high wavenumbers. Similar high-wavenumber instabilities were observed by other authors [34], [35], who used smoothing techniques to circumvent this difficulty. Here, at each time step Δt , we applied an ideal low-pass filter to η and ξ of the form

$$f(k) = \begin{cases} 1 & \text{if } |k|/k_{\max} \leq \nu, \\ 0 & \text{if } |k|/k_{\max} > \nu, \end{cases} \quad (20)$$

where k_{\max} is the highest wavenumber of the spectrum. We found that $\nu = 0.8$ suffices to stabilize the solution in most cases. Applying an ideal filter with a high value of ν ensures that only a very small amount of energy located in the high-wavenumber region of the spectrum is suppressed by filtering.

The performance of the code was assessed extensively by checking the accuracy of results (on wave profiles and conserved quantities) with respect to the different numerical parameters. For instance, we checked that a solitary wave of height $S = 0.3h$, generated by Tanaka’s method, propagates with negligible change of shape and speed up to $t = 1000\sqrt{h/g}$, with relative errors of only 10^{-7} and 5×10^{-7} in the conservation of the added mass $M(\eta_S)$ and the energy $H(\eta_S, \xi_S)$ respectively ($J = 8$, $N = 1024$, $\Delta t = 0.01\sqrt{h/g}$). For the head-on collision of two solitary waves of equal height $S = 0.3h$, we found that the added mass and the energy are conserved with a relative error of 6×10^{-8} and 2×10^{-7} respectively, up to $t = 90\sqrt{h/g}$ after collision.

D. Experimental setting

The experiments reported here have been conducted at the W.G. Prichard Fluid Mechanics Laboratory of Penn State University, in a precisely aligned glass wave channel of length 13.165 m and width 25.4 cm. The quiescent water depth for the experiments was 5.0 cm, within an accuracy of 0.25 mm (corresponding to a water volume in the channel accurate to one liter). Solitary waves were generated by the horizontal, piston-like motion of a paddle inserted in the channel cross-section, driven by a precision software controlled linear motor which allowed the generation of highly accurate and repeatable wave profiles. The measurements of the water surface were done by a bottom-mounted pressure transducer and by four non-contacting wave gages supported above the water surface on a traveling instrumentation carriage. Since

only four wave gages were available on the carriage, the water surface at only four spatial locations could be measured during a single experiment. The precision of the wavetank construction and the wavemaker driver made our experiments repeatable to within a high degree of accuracy. We used the sophistication of both the mechanical and the electronic systems under repetition of 40 experimental runs to produce a spatial profile that spans 1.6 m in the x -direction with a spatial resolution of 1 cm and a temporal resolution of 3.07 ms. A detailed presentation of the experimental procedures including the description of the wave channel and wave makers, the measurements and their analysis are given in Hammack, Henderson, Guyenne and Yi [36].

For head-on collisions of solitary waves, we generated KdV soliton profiles by specifying the paddle’s position and velocity, taking into account the finite motion of the wavemaker. Since only one wavemaker was available, it was necessary to produce a first solitary wave that propagated down the channel and reflected from the end wall. Subsequently, a second solitary wave was generated that collided with the reflected one near the center of the channel test section. The instrument carriage was fixed during each of these experiments.

In the case of co-propagating solitary waves, the wavemaker was used to create two KdV soliton profiles in rapid succession. Due to the relatively small differential velocity of the two solitary waves, the collision of a larger wave overtaking a smaller one occurs over a large distance down the wave channel. It is thus necessary to have the instrument carriage move in a frame of reference adapted to the mean velocity of the two waves. There was thus always a small uncertainty in the carriage position, especially during the acceleration and the deceleration periods of the experiment. This is discussed in Sec. VA when we compare experimental data and numerical simulations.

III. COUNTER-PROPAGATING SOLITARY WAVE COLLISIONS: SYMMETRIC CASE

The question at hand in this section and the following one concerns the details of the collision between two solitary waves traveling in opposite directions. In general counter-propagating solitary wave collisions, the solution is assumed to take the asymptotic form as $t \rightarrow -\infty$ of two clean solitary wave profiles moving towards one another, as in (17). During the collisions the solution rises to an amplitude larger than the sum of the amplitudes of the two incident solitary waves (the run-up). After the collision two similar principal waves emerge, with amplitudes which are initially significantly below their incident amplitudes, but which relax and regain amplitude again, returning to the form of two solitary waves, now separating from each other. As a result of this collision, the amplitudes of the two resulting solitary waves are slightly smaller than the incident amplitudes, their centers are

slightly retarded from the trajectories of the incoming centers (the phase lag), and there is a small residual. This asymptotic form as $t \rightarrow +\infty$ is as described in (18).

Because of the change of velocity after collision, there is a certain ambiguity surrounding the definition of the phase shift; indeed the solitary wave components have trajectories which are asymptotic to the lines $x = c_j t + a_j$, $j = 1, 2$ for $t \rightarrow -\infty$, and $x = c_j^+ t + a_j^+$, $j = 1, 2$ for $t \rightarrow +\infty$. To resolve the problem, define the midpoint of an interaction to be the time τ which minimizes the variance

$$V(t) = \int_{-\infty}^{\infty} (x - \frac{C}{M})^2 \eta dx ; \quad (21)$$

then the phase shift is well defined as the change in the $t = \tau$ intercept of these lines, namely $(a_j^+ - a_j) + \tau(c_j^+ - c_j)$, $j = 1, 2$.

The residual wave is supported between the two main solitary waves, and it propagates essentially according to linear theory, which among other things dictates that for large times after the collision, the residual is separated from the faster nonlinear solitary wave components of the solution. Thus this interaction has the form of a scattering event, with initial amplitudes (S_1, S_2) being transformed by the interaction to scattered amplitudes (S_1^+, S_2^+) and with a phase lag $(a_j - a_j^+) + \tau(c_j^+ - c_j)$, $j = 1, 2$ and radiative loss $\eta_R(x, t)$. It is a finite dimensional problem, with the scattering map $(S_1, S_2, a_1, a_2) \mapsto (S_1^+, S_2^+, a_1^+, a_2^+)$ and the residual $(\eta_R(x, t), \xi_R(x, t))$ being entirely determined by the two parameters (S_1, S_2) . For counter-propagating interactions, the major issues are: (i) to quantify the run-up as a function of initial amplitude and to compare it with previously derived results, (ii) to quantify the phase-lag $(a_j - a_j^+) + \tau(c_j^+ - c_j)$, $j = 1, 2$, (iii) to exhibit a residual after each collision and to examine its character, and (iv) to quantify the degree of inelasticity of such collisions by observing the changes in amplitude (analogously, the energy or the velocity) of the scattered solitary waves.

A. Run-up and phase lag

Our results for symmetric counter-propagating collisions between equal amplitude solitary waves consist in accurate numerical simulations of the initial value problem. Such interactions are equivalent to a single wave interacting with a vertical wall, although our calculations do not *a priori* impose symmetry on the solution. Two identical, well separated profiles $\eta_{S_j}(x - a_j)$, $j = 1, 2$ with opposing velocities $c_1 = -c_2$, which have been generated by Tanaka's method, are placed as initial data in the computational domain. In the nondimensional time interval of approximately 30 to 40 units they interact strongly, and then separate with a slight shift of phase and a slight change in amplitude. We display results for two different choices of amplitude: $S_j = \|\eta_{S_j}\|_{L^\infty} = 0.1h$ (Fig. 4) and

$S_j = \|\eta_{S_j}\|_{L^\infty} = 0.4h$ (Fig. 5). Fig. 4(a) [resp. Fig. 5 (a)] shows a collision between the solitary waves, with Fig. 4(b) [resp. Fig. (5b)] giving a space-time trace of the local maxima of this solution as the two individual crests merge and then separate in the process. At the attachment and detachment times of the individual crests, they propagate with infinite velocity. The asymptotically linear trajectories of the crests before and after collision can be compared to quantify the phase lag. Equivalently, Cooker, Weidman and Bale [4] use the wall residence time to quantify this degree of hesitation at the encounter of symmetric counter-propagating waves (a concept which is not available for asymmetric collisions).

Fig. 6 documents the time evolution of the maximum amplitude of the solution, which is shown to rise sharply to substantially more than twice the elevation of the incident solitary waves, after which it descends to below this level after crest detachment, relaxing back to almost its initial level. This is very comparable to Figs. 4(a) and (b) of Cooker, Weidman and Bale [4]. In Fig. 5 we observe that the phase lag grows when we increase the amplitude. Furthermore there is a residual clearly visible between the two crests after the collision.

For these and for a series of numerical simulations with a range of incident amplitudes from $0.025h$ to $0.5h$, values of run-up and wall residence time are recorded in Figs. 7 and 8 respectively, with comparison to the numerical data of Cooker, Weidman and Bale [4] and the asymptotic expressions to second and to third order as given in Byatt-Smith [7] and Su and Mirie [6], respectively. We also compare our observations of the wall residence time with the experiments of Maxworthy [5], as reported in Cooker, Weidman and Bale [4]. The experiments of Renouard, Seabra-Santos and Temperville [37] are consistent with this data. The very close fit between the results of Cooker, Weidman and Bale [4] and our own simulations represent a verification of the accuracy of the present numerical method, the only significant deviation occurring for calculated run-up in our largest amplitude case $S/h = 0.5$.

As noted in Cooker, Weidman and Bale [4], the asymptotic predictions of the phase lag in Oikawa and Yajima [8] and Su and Mirie [6] differ from the experiments of Maxworthy [5]; our numerical data are however almost indistinguishable from the numerical results of Cooker, Weidman and Bale [4], supporting again the latter case.

B. Residual

The residual is clearly visible trailing the main crests after the collision in the case $S_j = 0.4h$. In the case of smaller amplitude $S_j = 0.1h$, any deviation from a clean interaction is smaller than what can be seen under normal scaling. However an image of the interaction which appears in Fig. 9 with exaggerated vertical scale shows the presence of a small but definitive residual. In this and in our further simulations we have found that even

in the case of small to moderate amplitudes, there is always a non-zero energy transfer from the incident solitary waves to a residual, representing a qualitative confirmation of the asymptotic calculations of Su and Mirie [6] on this point. The transfer of energy from the solitary wave components results in a change in amplitude after passing through the interaction. In counter-propagating interactions, the amplitude of each solitary wave decreases, but by a remarkably small amount given the size of the incident solitary waves. We observe that relative amplitude loss is $(S - S^+)/S = 0.0036$ in the case $S = 0.1h$, while when $S = 0.4h$ the relative amplitude loss has only increased to 0.0065. Both of these changes are very small, which is qualitatively consistent with the findings of Su and Mirie [6] and Byatt-Smith [23], which predict no amplitude changes to orders $\mathcal{O}(S^3)$ and $\mathcal{O}(S^5)$ respectively. However our data show a quantitative discrepancy with both of these asymptotic predictions, which we will return to in section VI. We note that in the early simulations of Chan and Street [2] no residual was observed, up to the order of accuracy of the numerical simulation, and in Fenton and Rienecker [3] trailing residuals are only observed for large amplitude and symmetric counter-propagating interactions.

Table I gives the data from a sequence of numerical simulations of symmetric counter-propagating solitary wave interactions, with incident amplitudes $S = 0.025h$ through $0.5h$. We document two sets of quantities related to the inelastic character of interactions. The first is the change in amplitude of the solitary wave components passing through a collision $S/h \rightarrow S^+/h$, comparing it to the relative change $(S - S^+)/S$. The second is the total energy $E_T = H(\eta, \xi)$ of the solution compared with the energy of the residual $e_R = H(\eta_R, \xi_R)$. The residual is calculated by observing the best fit of the computed solution to two independent solitary waves (by matching amplitudes with numerically computed solitary wave profiles) at the given time t , and subtracting them from the solution. We additionally tabulate the relative energy loss of the two interacting solitary waves to the residual $e_R/H(\eta, \xi)$ that results from the collision.

Two facts are evident. Firstly, that there is in every case a non-zero energy transfer from the incident solitary waves to the residual as a result of the collision. And secondly that, although non-zero, the energy loss is very small; the relative loss varying from approximately 2% in the largest case $S/h = 0.5$, down to 0.5% when $S/h = 0.075$.

We now address the question of the fate of the solitary wave components after experiencing a collision and subsequent production of a residual. Our computations show that solitary waves emerging from a collision separate from each other *and* from the support of the residual wave generated by the collision, to propagate as clean solitary waves with slightly modified amplitude in an essentially quiescent background. In particular the collision lasts for a finite time, and only a finite portion of energy is lost in the interaction. It is a fact related to the sta-

bility of a solitary wave that, once perturbed, it does not continue to shed energy, even at a slow rate, as $t \rightarrow +\infty$. This is shown in the series of images in Fig. 10, in which two incident solitary waves of amplitude $S = 0.4h$ (a) approach each other, (b) collide and produce a residual, and (c) separate from the collision and from the support of the trailing wave packet which constitutes $(\eta_R(x, t), \xi_R(x, t))$. Given its amplitude and the background quiescent state in which it propagates, the residual wave evolves essentially according to linear theory. This figure also exhibits a characteristic teardrop shape of $\eta_R(x, t)$, resulting from the band-limited character of the residual and the dispersion relation $\omega^2(k) = gk \tanh(hk)$.

Fig. 11 presents a series of Fourier transforms of the residual $\eta_R(x, t)$ from the collision of two solitary waves of amplitude $S = 0.4h$, for a sequence of times $t/\sqrt{h/g} = 0.02, 13.20, 24.60, 42.90, 66.00$ and 89.10 . For reference, the Fourier transform of $\eta_S(x)$ is of amplitude 19.9870. In this sequence of Fourier profiles, Figs. 11(a) and 11(b) document the adjustment of the solution to its superposed solitary wave initial data. Fig. 11(c) represents the initial residual, well after the start of the numerical simulation, but well before the actual collision time. We observe that the solution has evidently relaxed to being very precisely a sum of two approaching solitary waves, as the amplitude of the Fourier transform of η_R is roughly three orders of magnitude smaller than the solitary wave components. Figs. 11(d)(e) and (f) document the Fourier signature of the residual at three stages after collision, when a characteristic oscillating and band-limited profile with two main lumps appears and stabilizes. At all times, the Fourier transform is essentially supported between wave numbers $k = \pm 2$. Under linear evolution, such a Fourier profile is preserved. This is consistent with the observation of the spatial profiles of the residual, namely that they are not highly oscillatory error terms, but rather they are of specific form with identifiable characteristics.

Fourier profiles of the development of the residual in other cases ($S = 0.1h, 0.2h, 0.3h$ and $0.5h$) show quite a degree of similarity with the sequence for the case $S = 0.4h$ in Fig. 11; we have not presented all of these data here.

IV. ASYMMETRIC COUNTER-PROPAGATING COLLISIONS

A. Experiments and numerical comparisons

Our results in the case of counter-propagating interactions between two solitary waves of unequal amplitudes include both experimental measurements and numerical simulations. The experiments, carried out in the Penn State wave channel, consist of a first localized waveform being generated by the wavemaker, reflecting off of the far end of the tank and then interacting with a second wave generated by the wavemaker. The water surface

level is measured in a spatial window around the region of collision at regular intervals of time. These two waveforms are generated to be profiles of a soliton solution of the KdV equation (and hence they are not strictly traveling wave solutions to the Euler equations, but only close). In addition, the reflected wave may well deviate further from an exact solitary wave profile due to the interaction with the wall, and experience a slight attenuation of amplitude due to its longer travel distance in the wavetank. Hence the interaction has a degree of asymmetry, and it is not strictly between exact solitary waves. Fig. 12 records the wavetank measurements of the experiments of this collision at eight times during the interaction, within a window located in the middle of the wave channel. The wavemaker and the end wall of the channel are not included in the image. In this figure, the wave moving from right to left is coming directly from the wavemaker, while the one moving from left to right has reflected from the end wall of the wave channel. The resulting measurements are compared with two numerically-generated traces, which are superimposed on the figure. The first is a numerical simulation of the water wave evolution using the above numerical methods to solve the time evolution problem (5) and (6). Initial data for this simulation are given to be KdV soliton profiles, matching those being generated in the tank by the wavemaker. The second is a linear superposition of two exact KdV solitons, centered on the two solitary-like waves present in Fig. 12(a) and adjusted to their amplitudes. Translating at constant (and opposing) velocity, they act as a reference for the amplitude and the phase shift of the actual solutions that are undergoing the interaction.

The details of the interaction in the experiment are relatively well represented in the numerical simulation, which in all frames predicts the measured wave profile with small error, and which reproduces the peak locations and their amplitudes very well. The two exceptions are that the numerical solution apparently slightly undershoots the measured wave amplitude at the point of largest run-up (Fig. 12(c)), and the centers of the peaks in the numerical solution are slightly delayed behind the experimental measurements after the interaction (Fig. 12(h)). Both clearly differ from the superposition of KdV solitons. Some of the unsteadiness in the experimental solution and the numerical simulation can be attributed to the fact that neither is starting from an exact solitary wave. Furthermore, neither a trailing residual nor any changes in amplitude due to the inelastic nature of the interaction can be picked out from the experimental uncertainties of the wavetank measurements.

B. Run-up, phase lag and residual

Further numerical simulations of counter-propagating interactions between two exact solitary waves of different amplitudes exhibit a number of the same features that have been observed in the symmetric case. Fig. 13 shows

the details of a collision between solitary waves of amplitudes $S_1 = \|\eta_{S_1}\|_{L^\infty} = 0.4h$ and $S_2 = \|\eta_{S_2}\|_{L^\infty} = 0.1h$. The clean propagation before the collision, the degree of run-up, the phase lag, and the small residual are clear in the two diagrams. The plot of the trajectories of the crests shows that the small solitary wave is absorbed by the larger, which subsequently slows briefly before re-emitting the smaller one on the other side and resuming (close to) its incident velocity. The phase lag is clearly asymmetric, with the smaller solitary wave being delayed more significantly than the larger.

Fig. 14 shows the similar behavior in an interaction between solitary waves of amplitudes closer to each other, respectively $S_1 = 0.4h$ and $S_2 = 0.3h$. In this case the run-up is more significant, as would be expected, the phase lag of the two solitary waves are comparable to each other, and the slowing of the central crest due to the interaction is significant. Additionally a larger residual is produced. Still however, judging from the trajectories of the two crests, the interaction has the character of an absorption of the smaller solitary wave, and its subsequent re-emission at a later time, along with a phase lag in their paths.

V. CO-PROPAGATING SOLITARY WAVE INTERACTIONS

A. Experiments and numerical comparison

Our results for the co-propagating case of interactions between two solitary waves include numerical simulations of these overtaking collisions, experimental measurements, and numerical modeling of the experiments. As in the case of head-on collisions, the solution is assumed to be in the asymptotic form as $t \rightarrow -\infty$ of two solitary waves infinitely separated from one another. In this case however these have velocity with the same sign, and are ordered so that initially the larger amplitude wave trails the smaller one. An overtaking collision consists of the larger solitary wave catching up with and interacting with the smaller one, subsequently passing on and separating from it, and leaving a residual ($\eta_R(x, t), \xi_R(x, t)$) trailing both of the resulting solitary waves. This is consistent on a qualitative level with the model interactions studied by Bona, Pritchard and Scott [15]. Because the interaction is occurring between solutions with velocities of the same sign, it takes place over a long time interval, in contrast to the case of the head-on collisions. The solitary waves resulting from the interaction have very slightly modified amplitudes and velocities, and they experience a substantial phase shift, which is positive (that is, their centers are advanced from where they would be had there not been an interaction). This is consistent with the phase shift for the interaction of KdV solitons, and opposite in sign to the case of head-on collisions. The major issues which involve these interactions are (i) to exhibit a residual wave

resulting from the inelastic nature of the interactions, and (ii) to quantify the changes in amplitude, energy and velocity due to the interaction $(S_1, S_2) \rightarrow (S_1^+, S_2^+)$; (iii) to quantify the phase shift $(a_j - a_j^+) + \tau(c_j^+ - c_j)$, $j = 1, 2$ and compare it with the analog quantity for KdV two-solitons; and (iv) to understand the changes in amplitude and other details of the dynamics of such interactions. As in the counter-propagating case, these interactions have the form of a scattering event, mapping (S_1, S_2, a_1, a_2) to $(S_1^+, S_2^+, a_1^+, a_2^+)$ and generating the residual $(\eta_R(x, t), \xi_R(x, t))$, all being determined by the two input parameters (S_1, S_2) .

Fig. 15 shows a sequence of spatial profiles taken of an experimental overtaking collision between two waves in the Penn State wave channel. Superposed on these profiles are two further traces; a sequence of spatial profiles predicted by our numerical simulations, and the KdV two-soliton which best fit the initial frame of the data. Initial data for the numerical simulations were chosen in a similar way to those for the head-on collision experiments; with superimposed KdV single solitons, as the wavemaker was programmed to produce these profiles. Experimental measurements are taken from a moving carriage above the wavetank, in order to keep the interaction within the frame of the instrument assembly. Because of uncertainties in the precise carriage position, we had difficulty aligning the reference frame of the experimental data and the two sets of numerical profiles. For this reason the sequence of profiles in Fig. 15 are calibrated to be at precisely the same *times* during the interaction, but they are plotted in the frame by individually aligning their respective centers of mass. Therefore amplitude and relative phase information is accurately reproduced, but absolute phase has been neglected.

One first notes that, while the shape of the experimental data and the numerical simulations are very well correlated throughout the interaction, the amplitude of the experiment decays in time and in the last frame in particular its amplitude is rather attenuated when compared to the simulation. The numerical simulation also over-predicts the phase shift after the interaction, especially that of the trailing wave. These two errors may be due to the presence of dissipative processes in the experiment that are not taken into account in the equations of motion (5)(6). These can be expected to play a greater rôle in overtaking interactions than in head-on collisions, as dissipative effects have more time to accumulate. These effects are discussed in detail in Weidman and Maxworthy [17], where experimental observations of overtaking solitary wave collisions are reported. On the other hand, the experiments are also compared to the KdV equation; one sees that the KdV two-soliton solution has overshoot the amplitude in almost all frames, and is giving a different picture of the crest interactions at the peak of the interaction. Overall, this result gives us a certain confidence in the predictive power of our numerical simulations.

B. Phase shift and bounds on amplitude

In a sequence of further numerical simulations, we have studied overtaking solitary wave collisions between moderate to large amplitude waves. In Figs. 16-19 we present the resulting space-time plots of the surfaces and the trajectories of the crests, in the cases of amplitudes $0.4h$ and $0.3h$, $0.4h$ and $0.1333\dots h$, 0.4 and $0.113h$, and $0.4h$ and $0.1h$ respectively. The plots are given in a coordinate frame moving approximately with the mean velocity of the two initial solitary waves, in order to localize the interaction into the frame of the image. One feature of all of these interactions is that there are large phase shifts $(a_j^+ - a_j) + \tau(c_j^+ - c_j)$, $j = 1, 2$, and that both of these quantities are positive. This is consistent with the phase shifts that occur in the KdV two soliton solution, although the actual values of the phase shifts for the KdV solitons are larger.

A second feature is that the scattering event amplifies the larger of the solitary waves. After the interaction, the larger solitary wave $\eta_{S_1^+}$ is of slightly larger amplitude than η_{S_1} , a phenomenon which has been reported previously in Fenton and Rienecker [3]. The data from our numerical simulations are given in Table II.

It is clearly seen that the amplitude increase is of 0.1% or less in all cases. This is an order of magnitude smaller than the changes in amplitude observed in counter-propagating interactions. We have to comment that while this is in qualitative agreement with the numerical study in [3] (of a single co-propagating interaction), our measurements differ quantitatively from their findings in that the increases $(S_1^+ - S_1)/h$ we observe are significantly smaller than that reported in their paper. The difference can perhaps be attributed to the higher precision of our numerics. A third feature of each of these interactions is that the amplitude of the actual solution $\eta(x, t)$ never exceeds that of the larger solitary wave, nor does it dip below the amplitude of the smaller. That is, at each time $t \in \mathbb{R}$, there is the estimate from above and below

$$\|\eta_{S_2}(x)\|_{L_x^\infty} < \|\eta(x, t)\|_{L_x^\infty} < \|\eta_{S_1^+}(x)\|_{L_x^\infty}, \quad (22)$$

where we are labeling the initial solitary waves so that $\|\eta_{S_2}(x)\|_{L_x^\infty} < \|\eta_{S_1}(x)\|_{L_x^\infty}$. This fact is verified in Fig. 20, in which the maximum of the solution is plotted in nondimensional time (solid line), with the upper and lower bounds $\|\eta_{S_1^+}(x)\|_{L_x^\infty}$ and $\|\eta_{S_2}(x)\|_{L_x^\infty}$ superimposed in horizontal dashed lines. The greatest dip in the amplitude of $\eta(x, t)$ occurs at the peak time of the interaction. This is in contrast to counter-propagating collisions, where the amplitude at the peak of the interaction experiences a run-up of a significant factor greater than the sum of the initial solitary waves. In the case of co-propagating interactions, the result is to lower the maximum at the peak of the interaction, and by a significant factor. In Figs. 20(a) and 20(b), the maximum dips below the arithmetic mean of the incoming amplitudes

$\frac{1}{2}(\|\eta_{S_1}(x)\|_{L^\infty} + \|\eta_{S_2}(x)\|_{L^\infty})$. In Fig. 20(c) the dip is not so exaggerated, but nevertheless it is significant. We recall for the reader that the estimate (22) also holds for KdV two-solitons.

C. Residual

What is not evident from the plots presented in Figs. 16, 17, 18 and 19 is the presence of a residual $\eta_R(x, t)$ emerging from the collision. In fact the residual exists, but it is very small; we have imaged it with an essentially 100-fold magnification in the scale of the vertical axis in Figs. 21 and 22. Fig. 21 plots the interaction of two solitary waves with $S_1 = 0.4h$ and $S_2 = 0.3h$, at three points in time. A small depression forms behind the two main peaks during the collision, which develops into a well defined but very small trailing residual as the two main solitary waves separate from the interaction. On this matter, Fenton and Rienecker [3] did not observe a residual in their simulations of overtaking collisions for the full Euler equations, up to the degree of precision of their calculation. We note that numerical observations of residuals resulting from an overtaking collision of solitary waves to model equations are well known [15], [11]. Fig. 22 is a similarly magnified plot of the simulation of an interaction between two solitary waves with $S_1 = 0.4h$ and $S_2 = 0.1h$ that appears in Fig. 19. Features of the residual $\eta_R(x, t)$ are qualitatively the same, but it possesses somewhat of a higher wavenumber spectrum. Again it is of an amplitude that is virtually undetectible in the non-magnified plot or in numerical simulations with less precision.

D. The Lax categories

A comparison between the different cases represented in Figs. 16, 17, 18 and 19 brings us to a discussion of the geometry of overtaking solitary wave collisions. We find that these interactions can be categorized into three types, closely related to the three Lax categories of two-soliton collisions for the KdV equation. When the amplitudes of the two incident solitary waves are close to being comparable, then the interaction looks like the one pictured in Fig. 16; namely at each point in time there are two well-defined and separate crests in the solution. The amplitude of the trailing crest is initially the larger S_1 , and it decreases monotonically through the interaction to the lower amplitude S_2^+ . The leading crest does the opposite, increasing monotonically in time. Throughout the interaction they never meet. This is the same behavior as the KdV two-solitons of category (a), as described in Lax [16]. In the situation that the amplitudes of the incident solitary waves are very different, the interaction looks like the one pictured in Fig. 19. As the two waves approach each other, the smaller crest is drawn towards the larger wave and absorbed by it, a process which ac-

celerates the crest of the larger wave. After a time interval during which there is a unique central crest, the smaller wave is re-emitted from the back of the principal wave, slightly modified in amplitude, after which it separates from the larger wave. This is the behavior of KdV two-soliton solutions in the Lax category (c) (except for the inelastic changes in amplitude). Between these two cases is an intermediate one, which for solitary wave interactions is pictured in Fig. 17. It is a more complicated picture; the smaller crest is first absorbed and then re-emitted from the larger wave, after which there is a central region consisting of two crests. In this region the smaller one grows while the larger shrinks until they have essentially traded their relative sizes; the interaction then undoes itself in a similar way. The pattern of crest absorption and re-emission is given in Fig. 17(b), and it is essentially identical to the interaction of KdV two-solitons in Lax' category (b). What is different for solitary waves solutions of Euler's equations is that the transitions occur for different values of the two incident amplitudes. For the KdV equation, when considering two-soliton interactions with amplitudes respectively $S_1 \geq S_2$, the transition from category (a) to (b) occurs at the ratio $S_1/S_2 = (3 + \sqrt{5})/2 \sim 2.62\dots$, and the transition from (b) to (c) when $S_1/S_2 = 3$. In the case of interactions of solitary waves, the transition curves between categories occur for different values of S_1 and S_2 , and are not simply functions of the amplitude ratio. In a series of trials with $S_1 = 0.4h$ and with varying S_2 , we have found that the transition value from category (a) to (b) and from (b) to (c) to be given by:

$$\begin{aligned} \frac{S_1}{S_2} &\leq 2.941 && \text{category(a)} && (23) \\ 2.941 &< \frac{S_1}{S_2} &\leq 3.536 && \text{category(b)} \\ 3.536 &< \frac{S_1}{S_2} && \text{category(c)} \end{aligned}$$

In the simulations presented in Figs. 16, 17 and 19 this ratio is 1.33\dots, 3 and 4 respectively. At the transition point from category (b) to (c) the central single crest at the peak of the interaction is just on the edge of splitting for an instant into two separated crests, and it apparently propagates with infinite velocity at this instant; this is captured in Fig. 18.

The appearance of three categories of two soliton interaction is an algebraic fact about the KdV equation, but it was not evident to us that co-propagating solitary wave interactions for the water waves problem would be so restricted. We made some attempt to find other geometric categories of interactions, for example between very large waves or between waves of very different amplitudes. However in all of our simulations, we found that the interactions fell within one of the three categories.

There have been previous studies which compare the Lax categories for KdV two-solitons with water waves. Weidman and Maxworthy [17] made experimental observations of overtaking collisions in the three categories.

Numerical simulations of overtaking collisions are reported by Mirie and Su [11] and Wu [18] for model long wave equations, and by Fenton and Rienecker [3] for Euler's equations. The latter reference also notes the shift in the transition boundaries for these categories, presenting a case of a category (b) overtaking interaction.

With this discussion in hand, we return to comment on the sequence of experimental measurements in Fig. 15. Noting that the amplitudes of the two incident waves are 0.730 cm and 2.295 cm respectively, their ratio is 3.14... , which for the KdV equation is of category (c). However for solitary waves it apparently falls well into the geometric category (b), and therefore a KdV two-soliton cannot be expected to be able to reproduce the detailed features of an overtaking collision in this regime. Considering the geometry of the wave profile, the numerical simulations of solitary waves observed in the laboratory do quite well in reproducing the evolving free surface in the experimental measurements in Fig. 15, despite the disagreements in the amplitudes due to the attenuation of the waves in the experiment.

The category of an interaction is observed to have an influence on the degree of inelasticity of the solitary wave interaction. Table II gives the data from a sequence of numerical simulations of co-propagating solitary wave interactions, where a wave of height $0.4h$ overtakes ones of height respectively $0.3h$, $0.1333h$, $0.113h$ and $0.1h$. We document the change in amplitude of the two component waves due to the collision, as well as the energy of the residual that is created as a result of the interaction. In all of our simulations, the larger solitary wave gains amplitude as a result of the interaction, at the expense of the smaller which loses amplitude. However it appears that this phenomenon does not change monotonically with the sizes of the two incident solitary waves. Furthermore the relative energy loss to the residual, which again is an order of magnitude smaller than that for counter-propagating interactions, is also not observed to be uniformly decreasing as the amplitude of the smaller wave decreases, at least over the range we have examined. It is apparent from the data that category (a) interactions are closer to being elastic, while category (b) and (c) interactions are less clean than those of category (a), and are more effective at transferring energy to the residual of the collision.

VI. AN ANALYSIS OF THE RESIDUAL

The purpose of this section is to present two relations satisfied by the residual $(\eta_R(x, t), \xi_R(x, t))$ resulting from a solitary wave collision. We show (i) there is a relationship between ΔS_j and the energy e_R carried by the residual, and (ii) we prove a rigorous estimate giving an upper bound for e_R . The estimate (ii) holds under the assumption that solitary wave collisions satisfy three hypotheses, which are observed to hold in our numerical simulations. However, we do not at present have a rigor-

ous proof of this fact, and they remain hypotheses of the result.

Our discussion of the residual is based on three conserved quantities: the added mass $M(\eta)$, the momentum $I(\eta, \xi)$ and the energy $H(\eta, \xi)$, defined respectively in (9), (10) and (7). Exact solitary wave profiles occur in one parameter families $(\eta_S(x - tc), \xi_S(x - tc))$, with $S \in [0, S_{max}]$. The solitary wave solutions have well defined values of the three conserved quantities, which we denote respectively $m(S) = M(\eta_S)$, $\mu(S) = I(\eta_S, \xi_S)$, and $e(S) = H(\eta_S, \xi_S)$. A solitary wave of amplitude S moving from left to right has positive momentum $\mu(S)$, while one of the same amplitude moving from right to left has identical mass $m(S)$ and energy $e(S)$, and negative momentum of the same absolute value.

We give initial data with asymptotic behavior for $t \rightarrow -\infty$ as in (17), so that the values of the total added mass, total momentum and total energy for our solution $(\eta(x, t), \xi(x, t))$ are given by

$$\begin{aligned} M_T &= m(S_1) + m(S_2) \\ I_T &= \mu(S_1) + \mu(S_2) \\ E_T &= e(S_1) + e(S_2) . \end{aligned} \quad (24)$$

Because they are conserved quantities, these values are preserved after an interaction, where we have observed that the solution takes the form (18), consisting of two separating solitary waves $(\eta_{S_1^+}, \xi_{S_1^+})$ and $(\eta_{S_2^+}, \xi_{S_2^+})$, with in addition a residual $(\eta_R(x, t), \xi_R(x, t))$.

Our first assumption, which we denote (H1) is that this will be the case in every binary solitary wave interaction; therefore after the interaction the conserved quantities can be calculated to be

$$\begin{aligned} M_T &= m(S_1^+) + m(S_2^+) + m_R \\ I_T &= \mu(S_1^+) + \mu(S_2^+) + \mu_R \\ E_T &= e(S_1^+) + e(S_2^+) + e_R . \end{aligned} \quad (25)$$

Taking the difference before and after the interaction gives us the relations

$$\begin{aligned} (m(S_1) - m(S_1^+)) + (m(S_2) - m(S_2^+)) &= m_R \\ (\mu(S_1) - \mu(S_1^+)) + (\mu(S_2) - \mu(S_2^+)) &= \mu_R \\ (e(S_1) - e(S_1^+)) + (e(S_2) - e(S_2^+)) &= e_R . \end{aligned} \quad (26)$$

Let $\Delta S_j = S_j - S_j^+$ for $j = 1, 2$; the mean value theorem implies that for $j = 1, 2$ there exist intermediate values $S_j^*(m)$, $S_j^*(\mu)$, and $S_j^*(e)$ in the intervals $[\min\{S_j^+, S_j\}, \max\{S_j^+, S_j\}]$ such that

$$\begin{aligned} m(S_j) - m(S_j^+) &= m'(S_j^*(m))\Delta S_j \\ \mu(S_j) - \mu(S_j^+) &= \mu'(S_j^*(\mu))\Delta S_j \\ e(S_j) - e(S_j^+) &= e'(S_j^*(e))\Delta S_j . \end{aligned} \quad (27)$$

To avoid overly clumsy notation we will write $m'(S_j^*(m)) = m'_j$, and similarly for μ'_j and e'_j . The three

relations (26) are rewritten

$$\begin{aligned} m'_1 \Delta S_1 + m'_2 \Delta S_2 &= m_R \\ \mu'_1 \Delta S_1 + \mu'_2 \Delta S_2 &= \mu_R \\ e'_1 \Delta S_1 + e'_2 \Delta S_2 &= e_R. \end{aligned} \quad (28)$$

In practice, the differences $\Delta S_j = S_j - S_j^+$ are very small, implying that the quantities m'_j , μ'_j and e'_j are very close to the values for the derivatives $m'(S_j)$, $\mu'(S_j)$, $e'(S_j)$ respectively, which are specified by the initial data.

In particular, in the symmetric counter-propagating case, we have $S := S_1 = S_2$, which implies by symmetry that $\Delta S := \Delta S_1 = \Delta S_2$ and $I_T = 0$ and $\mu_R = 0$. Equations (28) give relations between the mass and energy of the residual and the change in amplitude of the solitary waves due to the interaction;

$$2m' \Delta S = m_R, \quad 2e' \Delta S = e_R. \quad (29)$$

For small amplitudes S , solitary waves behave similarly to KdV solitons, and in particular their added mass, momentum and energy scale asymptotically in parallel with the KdV soliton profile $\eta_S \sim 2S \operatorname{sech}^2(\sqrt{S}x)$. That is,

$$\begin{aligned} m(S) &= M(\eta_S) \sim C_1 \sqrt{S} \\ \mu(S) &= I(\eta_S, \xi_S) \sim C_2 S^{3/2} \\ e(S) &= H(\eta_S, \xi_S) \sim C_3 S^{3/2}. \end{aligned} \quad (30)$$

Comparing this with our numerical simulations of solitary waves, Fig. 23 is a log-log plot showing the power law behavior of the energy of the solitary wave family through the range of solutions that we have generated using Tanaka's method; it is well matched to the power law $C_3 S^{3/2}$.

From (30) the asymptotic behavior of ΔS_j , $j = 1, 2$ and the quantities m_R , μ_R and e_R for small S_j are related. In the symmetric case, equations (29) determine the relationship

$$\begin{aligned} C_1 S^{-1/2} \Delta S &= m_R \\ 3C_3 S^{1/2} \Delta S &= e_R \end{aligned} \quad (31)$$

between the asymptotic behavior of ΔS and the quantities m_R and e_R as $S \rightarrow 0$.

A. Estimates of the residual

To continue this analysis, we make a second assumption (H2), that for sufficiently large time t^+ after the interaction, the two solitary wave components of the resulting solution are well separated both from each other and essentially from the support of the residual (as observed in Fig. 10). Therefore because $(\eta_{S_1^+}, \xi_{S_1^+})$ and $(\eta_{S_2^+}, \xi_{S_2^+})$ are small where $\eta_R(x, t)$ is important, we have

$$m_R = M(\eta_R), \quad \mu_R = I(\eta_R, \xi_R), \quad e_R = H(\eta_R, \xi_R). \quad (32)$$

The relation (28) can then be used to form an estimate for the residual term. Our considerations are divided into three cases.

1. Symmetric counter-propagating case

In this instance, solutions satisfy $I_T = 0$ and $I_R = 0$, which also implies that $\Delta S_1 = \Delta S_2$. Equations (29) imply that

$$e_R = \beta(S) m_R \quad \text{for} \quad \beta(S) = \frac{e'}{m'} \sim \frac{\partial e}{\partial m}(S). \quad (33)$$

Given the condition (H2) that the residual is essentially separated from the two scattered solitary waves, this states that $H(\eta_R, \xi_R) = \beta(S_1) M(\eta_R)$, which is to say that

$$\frac{1}{2} \int \xi_R G(\eta_R) \xi_R + g \eta_R^2 dx = \beta(S) \int \eta_R(x, t) dx. \quad (34)$$

After the interaction at a time t^+ at which the assumption (H2) holds, the two solitary wave components are separated by a distance $2L$.

We will further assume (H3) that the principal contribution to the residual, in the counter-propagating case, lies within the interval $(-L, L)$ (as is clearly shown in Fig. 10). The identity (34) gives rise to an estimate for the residual over this interval; indeed the Cauchy-Schwartz inequality implies

$$\int_{-L}^L \eta_R(x, t^+) dx \leq \sqrt{2L} \left(\int_{-L}^L \eta_R^2(x, t^+) dx \right)^{1/2}. \quad (35)$$

Used in the relation (34) this implies that

$$\begin{aligned} \frac{g}{2} \int_{-L}^L \eta_R^2(x, t^+) dx \\ \leq \beta(S) \sqrt{2L} \left(\int_{-L}^L \eta_R^2(x, t^+) dx \right)^{1/2}, \end{aligned} \quad (36)$$

which is to say that there is a bound on the potential energy of the residual;

$$\left(\int_{-L}^L \eta_R^2(x, t^+) dx \right)^{1/2} \leq \frac{2\beta(S)}{g} \sqrt{2L}. \quad (37)$$

Using this in the relation (34) for a second time gives control of the kinetic energy as well, that is;

$$\begin{aligned} \frac{1}{2} \int \xi_R G(\eta_R) \xi_R + g \eta_R^2 dx \\ \leq \beta(S) \sqrt{2L} \left(\int_{-L}^L \eta_R^2(x, t^+) dx \right)^{1/2} \leq \beta^2(S) \frac{4L}{g}. \end{aligned} \quad (38)$$

This estimate is valid throughout the parameter range for which our hypotheses (H1), (H2) and (H3) hold. From our numerical simulations we anticipate that they will hold for at least $0.025 \leq S \leq 0.5h$.

Estimate (38) gives rise to a quantitative bound on the residual in the setting of interactions between small solitary waves. From (30) we have that $e(S) \sim C_4 m^3(S)$ and therefore $\beta(S) = \partial_m e \sim C_5 m^2$. We conclude that,

at least for small initial amplitudes S , the energy carried from the interaction by the residual is bounded above by

$$H(\eta_R, \xi_R) \leq \beta^2(S) \frac{6L}{g} \leq C_6 S^2 . \quad (39)$$

i.e. energy loss due to inelastic collisions is bounded above by the second power of amplitude. The relative energy loss in this case is bounded by

$$H(\eta_R, \xi_R)/E_T \leq C_7 S^{1/2} . \quad (40)$$

2. General counter-propagating case

The general case follows an argument along similar lines. Expression (28) gives three equations for the two unknowns ΔS_1 and ΔS_2 . This implies that there is an additional relation between the quantities m_R , μ_R and e_R , which in turn can give rise to information on the residual (η_R, ξ_R) . One checks that the function $\partial_m \mu(S)$ is monotone increasing (indeed Fig. 3 shows that the impulse as a function of the mass increases faster than linearly, at least over the interval $0 \leq S/h < 0.5$ which covers all of our experiments and numerical simulations) which implies that system (28) can be solved for $(\Delta S_1, \Delta S_2)$ as a function of (m_R, μ_R) . The result gives an explicit extra relation between the conserved quantities for the residual, in the form

$$e_R = \alpha(S_1, S_2) \mu_R + \beta(S_1, S_2) m_R . \quad (41)$$

Assuming that (H2) is valid, this is the identity

$$\begin{aligned} & \frac{1}{2} \int \xi_R G(\eta_R) \xi_R + g \eta_R^2 dx \\ &= \alpha(S_1, S_2) \int \eta_R \partial_x \xi_R dx + \beta(S_1, S_2) \int \eta_R(x, t) dx . \end{aligned} \quad (42)$$

Under the Galilean transformation $(x, \xi_R) \rightarrow (x - t\Delta c, \xi_R - x\Delta c)$ this becomes

$$\begin{aligned} & \frac{1}{2} \int \xi_R G(\eta_R) \xi_R + g \eta_R^2 dx \\ &= (\alpha - \Delta c) \int \eta_R \partial_x \xi_R dx \\ & \quad + \left(\beta + \alpha \Delta c - \frac{(\Delta c)^2}{2} \right) \int \eta_R(x, t) dx . \end{aligned} \quad (43)$$

Making the choice of $\Delta c = \alpha$, we then have

$$\begin{aligned} & \frac{1}{2} \int \xi_R G(\eta_R) \xi_R + g \eta_R^2 dx \\ &= \left(\beta + \frac{\alpha^2}{2} \right) \int \eta_R(x, t) dx . \end{aligned} \quad (44)$$

We denote by $\beta' = \beta + \frac{\alpha^2}{2}$ the result of the Galilean coordinate transformation. In the asymmetric counter-propagating case, relying upon assumption (H3) that the

most important component of the residual lies between the two scattered solitary waves, and using the line of argument above, the deduction is that the energy of the residual is bounded;

$$\frac{1}{2} \int \xi_R G(\eta_R) \xi_R + g \eta_R^2 dx \leq (\beta'(S_1, S_2))^2 \frac{4L}{g} . \quad (45)$$

Consider small amplitude interactions, for $|S| \ll 1$ we parametrize $S_1 = a_1 S$, $S_2 = a_2 S$, with the difference $a_2 - a_1 \sim S$. Then an estimate analogous to (39) shows that

$$H(\eta_R, \xi_R) \leq (\beta'(S))^2 \frac{4L}{g} \leq C_8 S^2 , \quad (46)$$

and similarly for the relative error in (40). When $a_2 - a_1 = \mathcal{O}(1)$ more accurate rigorous upper estimate would be of interest.

3. Co-propagating case

Finally, in the co-propagating case, the numerical simulations clearly show the residual to be trailing both of the scattered solitary waves $\eta_{S_1^+}$ and $\eta_{S_2^+}$. We replace the assumption (H3) with its analog for this situation, namely (H3') that the principal contribution to the residual η_R remains in motion in the same direction as the solitary waves themselves. The rôle of the interval $[-L, L]$ in the analysis is replaced by the interval $[0, L']$, where at time t^+ after the interaction L' is sufficiently large for this interval to contain the most important component of (η_R, ξ_R) . The extra identity derived from (28) is similar in character to (45). We note that the interval $[-L, L]$ in the counter-propagating case is relatively short, as the dynamics of a head-on collision are a rapid process. Overtaking collisions on the other hand take a long time to complete, and therefore we expect that the interval $[0, L']$ is substantially longer, and the estimate analogous to (46) in this case is weaker since the overall constant factor is larger.

B. Comparison with data

We focus on the case of symmetric counter-propagating interactions, comparing the data in Table I with the relation (29). Fig. 24 is a log-log plot of the data in column 3 of Table I, representing the change in amplitude of a solitary wave due to a symmetric head-on collision. The data fit a power law $\Delta S \sim \gamma_1 (S/h)^{p_1}$ with $p_1 = 1.5$ and $\gamma_1 = 1.05 \times 10^{-2}$. There are two exceptional points, corresponding to $S = 0.025h$ and $S = 0.05h$, which overestimate $\Delta S/h$ to some extent (by 5×10^{-5} and 6×10^{-5} respectively). This is possibly related to the fact that the solitary waves emerging from a collision of this form have amplitudes lower than their asymptotic values, and require a certain relaxation time to reach them. For collisions of small amplitude waves, the relaxation time is

very long, and our measurements of the amplitudes S_j^+/h are possibly taken before the time at which the solution has effectively achieved its final state up to the accuracy of the simulation.

Fig. 25 is a log-log plot of the total energy of the residual e_R . The data fit a power law in the form $e_R \sim \gamma_2(S/h)^{p_2}$ with $p_2 = 2$, and $\gamma_2 = 5 \times 10^{-2}$. The same two data points $S = 0.025h$, $S = 0.05h$ are again measured slightly larger than the linear fit to the bulk of the data (by similarly small amounts), for what seems to us to be the same reason. We note that p_1 and p_2 satisfy the relationship indicated by (31) as required, namely $p_2 = p_1 + 1/2$. We further note that, while the estimate (39) is simply an upper bound on the energy of the residual, our observations are that it scales in powers of the amplitude S/h in an optimal manner as $S/h \rightarrow 0$.

With this data, the reasoning for small residual and amplitude changes is not from a high order effect in powers of S/h , rather it can be attributed as a consequence of the constants γ_j , $j = 1, 2$ being very small.

These findings are at odds with Su and Mirie [6] and Byatt-Smith [23], who predict that a residual is generated by the interaction only at order $\mathcal{O}((S/h)^3)$ in an asymptotic expansion, with the result that the energy of the residual is $e_R = \mathcal{O}((S/h)^{11/2})$. They also predict that the changes in amplitude are $\Delta S = o((S/h)^3)$. Using the relation (31), this behavior of e_R implies that in fact $\Delta S = \mathcal{O}((S/h)^5)$. Both of these predictions disagree with the data from our simulations over the range $(S/h) \in [0.025, 0.5]$. Two of the possible reasons for this difference are that (1) the regime of validity of the asymptotic expansion in [6] is limited to values of S/h smaller than those in the range of our simulations, or (2) the asymptotic analysis of [6, 23] predict well the initiation of a wave collision, but represent less well the detailed dynamics during the height of the collision, and the subsequent separation of the solution into two solitary waves plus residual. This latter possibility would also account for the fact that [6] predicts very well the run-up of a solitary wave collision, but less well the later details of the interaction, see Fig. 8.

C. Discussion of previous rigorous results

There are a certain number of rigorous results on the approximation of general solutions of the problem of surface water waves by solutions of model equations. In particular the KdV equation plays a rôle when the initial data are taken to be in the form of $\eta_0(x) = \varepsilon^2 q(\varepsilon x)$, $\xi_0(x) = \varepsilon p(\varepsilon x)$ for sufficiently small $\varepsilon = \sqrt{S/h}$, which is the appropriate scaling for the long-wave limit. This has a bearing on the problem of solitary wave collisions when the initial data consists of two KdV solitons, as they are taken to approximate the interaction. An initial step in this direction appears in Craig [19], where the result is a justification of the use of solutions of the KdV equation to approximate solutions of the water wave

problem in two space dimensions. The work of Schneider and Wayne [20] extends [19], allowing for solitary wave initial data, and for the phenomenon that data for the water wave problem, adapted suitably to the scaling of the KdV regime (and somewhat localized) breaks up into an essentially left-moving component and an essentially right-moving component as time evolves, with each of these components being well approximated by solutions of two decoupled KdV equations,

$$\begin{aligned} -2\partial_T q^- &= \frac{1}{3}\partial_{X_-}^3 q^- + 3q^- \partial_{X_-} q^- \\ 2\partial_T q^+ &= \frac{1}{3}\partial_{X_+}^3 q^+ + 3q^+ \partial_{X_+} q^+, \end{aligned} \quad (47)$$

where $X_\pm = \varepsilon(X \pm t)$ and X is a Lagrangian spatial coordinate in long-wave scaling. Rigorous theorems on the higher order corrections to the approximation given by the KdV equation are given in recent papers of Wright [22] and Bona, Colin and Lannes [21], following prior work of Wayne and Wright [38] on the Boussinesq and KdV models. The corrections derived in the former paper consist of two linearized KdV equations, one for each direction of propagation, and an inhomogeneous wave equation coupling the two KdV equations. In [22] these are

$$\begin{aligned} -2\partial_T f^- &= \frac{1}{3}\partial_{X_-}^3 f^- + 3\partial_{X_-}(q^- f^-) + J^- \\ 2\partial_T f^+ &= \frac{1}{3}\partial_{X_+}^3 f^+ + 3\partial_{X_+}(q^+ f^+) + J^+ \\ \partial_\tau^2 p - \partial_X^2 p &= 3\partial_X^2 \left(q^-(X - \tau, \varepsilon^2 \tau) q^+(X + \tau, \varepsilon^2 \tau) \right). \end{aligned} \quad (48)$$

The functions J^\pm are explicit nonlinear expressions in q^\pm and their derivatives. These corrections enter the solution at order $\mathcal{O}(\varepsilon^4) = \mathcal{O}((S/h)^2)$, and the rigorous Sobolev bounds on the resulting higher order error are of order $\mathcal{O}(\varepsilon^{11/2}) = \mathcal{O}((S/h)^{11/4})$. In the case of solitary wave collisions, the rôle of this inhomogeneous wave equation is essentially to describe the residual, and its order of magnitude is consistent with our error bounds above. For it to be consistent with the results of [6], the correction p would have to vanish. Of course these results are only valid for small ε .

VII. CONCLUSIONS

The results in this paper include experimental measurements of precisely generated solitary wave interactions, accurate numerical simulations of such collisions, and an analytic result on their scattering which gives an upper bound on energy loss to the inelastic nature of the collision process. In a first sequence of numerical simulations of counter-propagating interactions between identical solitary waves, we reproduce the findings of Cooker, Weidman and Bale [4] using our independent methods, thereby providing a validation of our numerical approach

and giving a verification of their as well as our own findings. Elements of the comparison include measurements of the run-up and wall residence time of collisions. Our numerical results on run-up are consistent with the predictions of Su and Mirie [6], while our results on the wall residence time are very close to those of Cooker, Weidman and Bale [4], which deviate from the expressions given in the former article. Both the latter reference and our results correspond to the experimental observations in Maxworthy [5].

In addition, the accuracy of our numerical simulations allows us to quantify the degree of inelasticity of these symmetric solitary wave collisions, which we have found to be very small but nonetheless nonzero in all cases we have examined. In the case of counter-propagating interactions between solitary waves of different sizes, we have taken the wavetank data from head-on solitary wave collisions and compared it with matched numerical simulations, finding that the run-up, the phase lag and as well the details of the geometry of the numerical solitary wave collisions predict quite accurately the measurements taken of the experiments. With this confidence in the precision of our numerical methods, the simulations allow us to measure the changes in mass, momentum and energy, as well as amplitude and velocity, of solitary waves due to an inelastic head-on collision. The resulting residual wave possesses a characteristic-shaped oscillatory profile, and it propagates essentially as a solution of the linear equations, at least subsequent to a point in time somewhat after the collision. The post-collision solitary waves exhibit strong evidence of stability, propagating away from the residual and leaving an interval of quiescent water surface between itself and the residual. The existence of a residual is qualitatively consistent with the asymptotic predictions of Su and Mirie [6] and Byatt-Smith [23]. However on a quantitative level our numerical data are at odds with their findings. In all cases we observed, both solitary waves exit from the collision with amplitudes slightly smaller than their entering values, with the amount of this change being directly related to the energy carried away from the collision by the residual.

Our observations and numerical simulations of co-propagating solitary wave interactions provide insight into this class of overtaking collisions. Again in all cases we observe the formation of a residual, in these cases trailing behind the smaller of the solitary waves after the collision. However this residual is typically even less pronounced than in the counter-propagating case. Additionally, we observed that the larger solitary wave exits from an interaction with slightly increased amplitude, while the smaller one loses amplitude. While counter-propagating collisions resulted in the maximum amplitude of the solution (the run-up) being substantially more than the sum of the entering solitary wave amplitudes, co-propagating collisions are of a very different character; in all cases the maximum of the solution does not exceed the maximum among the amplitudes of the two incident

and the two resulting solitary waves from the collision (which we find to be the amplitude of the largest exiting solitary wave). Nor does the maximum of the solution at any time lie below the minimum of the amplitudes of the four involved solitary waves.

We further find that interactions between co-propagating solitary waves fit very neatly into the three geometrical categories introduced by Lax [16] to describe two-soliton solutions of the KdV equation. However the transition points between the categories for solitary waves are not identical to their values for the KdV equation. This difference serves to explain in part the good fit between the experimental observations of co-propagating solitary wave interactions and the numerical simulations, and the discrepancies between both of these and the KdV approximation to the interaction. We have also found that the category of a solitary wave interaction influences the degree to which it is inelastic; category (a) interactions are apparently very close to elastic, while interactions in categories (b) and (c) are more effective in generating a residual.

Under three hypotheses on the nature of a solitary wave collision, we formulate a rigorous result for an upper bound on the energy loss in a solitary wave collision due to its inelastic nature. The hypotheses are essentially that (*H1*) solitary wave collisions are binary interactions and result in two exiting solitary waves plus a residual, (*H2*) in the regime of amplitudes considered, solitary waves are stable (to two dimensional perturbations caused by collisions), and (*H3*) the residual lies essentially in the expected region of the free surface. From these assumptions, using the conservation of added mass, momentum and energy, we derive an upper bound on the possible energy transfer to the residual from a collision. For small amplitude counter-propagating interactions, this estimate is seen to give the sharp order of magnitude for the energy of the residual.

Acknowledgments

The research in this paper has been partially supported by the NSF-Focused Research Group grant # DMS-0139847. In addition, the work of WC has been supported by the Canada Research Chairs Program and the NSERC through grant # 238452-01; the work of PG has been partially supported by a SHARCNET Postdoctoral Fellowship; the work of JH and DH has been partially supported by the NSF under # DMS-0139847; and the work of CS has been partially supported by the NSERC through grant # 46179-05. We thank S. Grilli for his coded version of the Tanaka method, and D. Nicholls for his numerical routines related to surface spectral methods. We also thank the anonymous referee for his/her comments on the first version of formulae (30), which led us to re-evaluate the conclusions of Su and Mirie [6] in the light of our numerical data and rigorous results. Computer simulations have been performed on the computing

Joe Hammack passed away suddenly on September 10, 2004, when the research in this manuscript was in progress. We very much miss his contributions to our collaboration, and we acknowledge with gratitude his deep insight and his always gracious comments during the course of our work.

APPENDIX: MODIFIED TANAKA'S METHOD

Tanaka's method for computing exact solitary waves is based on Cauchy's integral theorem for the complex velocity potential, in a reference frame moving with the wave speed c . The crest velocity V_c fully defines the wave field and the dimensionless crest velocity $q_c = V_c/c$ is used as a parameter in the problem. The original method by Tanaka [9] was modified by Cooker [39] to use the wave height S instead of q_c as a parameter. We propose here a modified version which is based on an alternate integral formulation.

Following Tanaka [9], we introduce the complex velocity potential $W = \varphi + i\psi$, choosing $\varphi = 0$ at the crest and $\psi = 0$ at the flat bottom. The fluid region is mapped onto the strip $0 < \psi < 1$, $-\infty < \varphi < \infty$ in the W -plane with $\psi = 1$ corresponding to the free surface. We also introduce the quantity $\Omega = \ln(dW/dz)$, where $z = x + iy$ (x being the horizontal coordinate and y the vertical one pointing upward). In terms of the magnitude q of the velocity and the angle θ between the velocity and the x -axis, Ω can be expressed as $\Omega = \tau - i\theta$ with $\tau = \ln q$. Throughout the fluid region, Ω is an analytic function of z and W , which tends to zero at infinity.

The Bernoulli condition at the free surface and the kinematic condition at the bottom can then be expressed as

$$\frac{dq^3}{d\varphi} = -\frac{3}{F^2} \sin \theta \quad \text{on} \quad \psi = 1, \quad (\text{A.1})$$

and

$$\theta = 0 \quad \text{on} \quad \psi = 0, \quad (\text{A.2})$$

respectively, where $F = c/\sqrt{gh}$ is the Froude number.

The problem of finding solitary wave solutions is thus transformed into the problem of finding a complex valued function Ω that is analytic with respect to W within the unit strip $0 < \psi < 1$, that decays at infinity, and satisfies the two boundary conditions (A.1) and (A.2). This can be done by iteration.

The main steps in the iterative procedure are as follows:

1. Fix an initial guess for $0 < q_c < 1$ and $\tau(\varphi)$, such that $\tau(0) = \ln q_c$ and $\tau(\infty) = 0$.
2. Compute the singular integral

$$-\theta(\varphi) = PV \int_{-\infty}^{\infty} \frac{\tau(\varphi')}{2 \sinh\left(\frac{\pi(\varphi' - \varphi)}{2}\right)} d\varphi', \quad (\text{A.3})$$

for $\theta(\varphi)$ (see Woods [40]). This formulation of $\theta(\varphi)$ (involving the Hilbert transform for a fixed strip) is completely equivalent to that in the original method. However it is computationally more efficient, as it does not require to solve a linear system for $\theta(\varphi)$ at each iteration and only one integral needs to be evaluated instead of three integrals (see Equation (3) in Tanaka [9]).

3. Integrate to find F^2 from $\theta(\varphi)$;

$$1 - q_c^3 = -\frac{3}{F^2} \int_0^\infty \sin \theta(\varphi) d\varphi. \quad (\text{A.4})$$

4. Evaluate

$$q^3(\varphi) - q_c^3 = -\frac{3}{F^2} \int_0^\varphi \sin \theta(\varphi') d\varphi', \quad (\text{A.5})$$

to find $q^3(\varphi)$ from $\theta(\varphi)$ and F^2 .

5. Determine new $\tau(\varphi) = \ln q(\varphi)$.
6. Repeat steps (b)–(e) until convergence is achieved for F^2 .

The wave profile and velocity potential are determined from the free surface velocity. As in Tanaka [9], for the calculation of steep solitary waves, the variable transformation

$$\varphi = \alpha\gamma + \gamma^m, \quad (\text{A.6})$$

is introduced, where α is a positive real number and m a positive odd integer. Lagrangian interpolation and trapezoidal rule are used to evaluate numerically the integrals in (A.3), (A.4) and (A.5). Typically, for $S = 0.4h$, $\alpha = 0.01$, $m = 5$ and a convergence criterion on F^2 equal to 10^{-10} , it was found that 60 iterations are necessary to achieve convergence. This is essentially the same number of iterations as required by Tanaka's original method.

[1] G. G. Stokes, "On the theory of oscillatory waves," Trans. Camb. Phil. Soc. **8**, 441 (1847).
 [2] R. K.-C. Chan, and R. Street, "A computer study of

finite amplitude water waves," J. Comput. Phys. **6**, 68 (1970).
 [3] J. D. Fenton, and M. M. Rienerker, "A Fourier method

- for solving nonlinear water-wave problems: application to solitary-wave interactions,” *J. Fluid Mech.* **118**, 411 (1982).
- [4] M. J. Cooker, P. D. Weidman, and D. S. Bale, “Reflection of a high-amplitude solitary wave at a vertical wall,” *J. Fluid Mech.* **342**, 141 (1997).
- [5] T. Maxworthy, “Experiments on the collision between two solitary waves,” *J. Fluid Mech.* **76**, 177 (1976).
- [6] C. H. Su, and R. M. Mirie, “On head-on collisions between two solitary waves,” *J. Fluid Mech.* **98**, 509 (1980).
- [7] J. G. B. Byatt-Smith, “An integral equation for unsteady surface waves and a comment on the Boussinesq equation,” *J. Fluid Mech.* **49**, 625 (1971).
- [8] M. Oikawa, and N. Yajima, “Interaction of solitary waves - a perturbation approach to nonlinear systems,” *J. Phys. Soc. Japan* **34**, 1093 (1973).
- [9] M. Tanaka, “The stability of solitary waves,” *Phys. Fluids* **29**, 650 (1986).
- [10] W. Craig, and C. Sulem, “Numerical simulation of gravity waves,” *J. Comput. Phys.* **108**, 73 (1993).
- [11] R. M. Mirie, and C. H. Su, “Collisions between solitary waves,” *J. Fluid Mech.* **115**, 475 (1982).
- [12] J. L. Bona, and M. Chen, “A Boussinesq system for two-way propagation of nonlinear dispersive waves,” *Physica D* **116**, 191 (1998).
- [13] J. Hammack, and H. Segur, “The Korteweg–de Vries equation and water waves: Part 2. Comparison with experiment,” *J. Fluid Mech.* **65**, 289 (1974).
- [14] Q. S. Zou, and C. H. Su, “Overtaking collision between two solitary waves,” *Phys. Fluids* **29**, 2113 (1986).
- [15] J. L. Bona, W. G. Pritchard, and L. R. Scott, “Solitary-wave interaction,” *Phys. Fluids* **23**, 438 (1980).
- [16] P. D. Lax, “Integrals of nonlinear equations of evolution and solitary waves,” *Comm. Pure Appl. Math.* **21**, 467 (1968).
- [17] P. D. Weidman, and T. Maxworthy, “Experiments on strong interactions between solitary waves,” *J. Fluid Mech.* **85**, 417 (1978).
- [18] T. Y. Wu, “Nonlinear waves and solitons in water,” *Physica D* **123**, 48 (1998).
- [19] W. Craig, “An existence theory for water waves and the Boussinesq and Korteweg–de Vries scaling limits,” *Comm. Part. Diff. Eq.* **10**, 787 (1985).
- [20] G. Schneider, and C. E. Wayne, “The long-wave limit for the water wave problem. I. The case of zero surface tension,” *Comm. Pure Appl. Math.* **53**, 1475 (2000).
- [21] J. L. Bona, T. Colin, and D. Lannes, “Long wave approximations for water waves,” Preprint (2005).
- [22] J. D. Wright, “Corrections to the KdV approximation for water waves,” *SIAM J. Math. Anal.*, In press.
- [23] J. G. B. Byatt-Smith, “The reflection of a solitary wave by a vertical wall,” *J. Fluid Mech.* **197**, 503 (1988).
- [24] V. E. Zakharov, “Stability of periodic waves of finite amplitude on the surface of a deep fluid,” *J. Appl. Mech. Tech. Phys.* **9**, 190 (1968).
- [25] R. Coifman, and Y. Meyer, “Nonlinear harmonic analysis and analytic dependence,” *AMS Proc. Symp. Pure Math.* **43**, 71 (1985).
- [26] W. Craig, P. Guyenne, D. P. Nicholls, and C. Sulem, “Hamiltonian long wave expansions for water waves over a rough bottom,” *Proc. R. Soc. A* **461**, 839 (2005).
- [27] W. Craig, P. Guyenne, and H. Kalisch, “Hamiltonian long wave expansions for free surfaces and interfaces,” to appear in *Comm. Pure Appl. Math.*
- [28] P. Guyenne, and D. P. Nicholls, “Numerical simulation of solitary waves on plane slopes,” *Math. Comput. Simul.* **69**, 269 (2005).
- [29] J. G. B. Byatt-Smith, and M. S. Longuet-Higgins, “On the speed and profile of solitary waves,” *Proc. R. Soc. London, Ser. A* **350**, 175 (1976).
- [30] J. Hunter, and J.-M. Vanden-Broeck, “Solitary and periodic gravity-capillary waves of finite amplitude,” *J. Fluid Mech.* **134**, 205 (1983).
- [31] D. P. Nicholls, “Traveling water waves: spectral continuation methods with parallel implementation,” *J. Comput. Phys.* **143**, 224 (1998).
- [32] M. Frigo, and S. G. Johnson, “The fastest Fourier transform in the West,” MIT-LCS-TR-728, available at <http://theory.lcs.mit.edu/fftw/>.
- [33] W. J. D. Bateman, C. Swan, and P. H. Taylor, “On the efficient numerical simulation of directionally spread surface water waves,” *J. Comput. Phys.* **174**, 277 (2001).
- [34] M. S. Longuet-Higgins, and E. D. Cokelet, “The deformation of steep surface waves on water. I. A numerical method of computation,” *Proc. R. Soc. London, Ser. A* **350**, 1 (1976).
- [35] D. G. Dommermuth, and D. K. P. Yue, “A high-order spectral method for the study of nonlinear gravity waves,” *J. Fluid Mech.* **184**, 267 (1987).
- [36] J. Hammack, D. Henderson, P. Guyenne, and M. Yi, “Solitary-wave collisions,” *Proc. ASME Offshore Mechanics and Arctic Engng*, (A symposium to honor Theodore Yao-Tsu Wu) Vancouver, Canada, June 2004, *World Scientific*.
- [37] D. P. Renouard, F. J. Seabra-Santos, and A. M. Temperville, “Experimental study of the generation, damping and reflexion of a solitary wave,” *Dyn. Atmos. Oceans* **9**, 341 (1985).
- [38] C. E. Wayne, and J. D. Wright, “Higher order modulation equations for a Boussinesq equation,” *SIAM J. Appl. Dyn. Syst.* **1**, 271 (2002).
- [39] M. Cooker, “The interaction between steep water waves and coastal structures,” PhD thesis, University of Bristol, UK, 1990.
- [40] L. C. Woods, *The theory of subsonic plane flow* (Cambridge University Press, 1961).

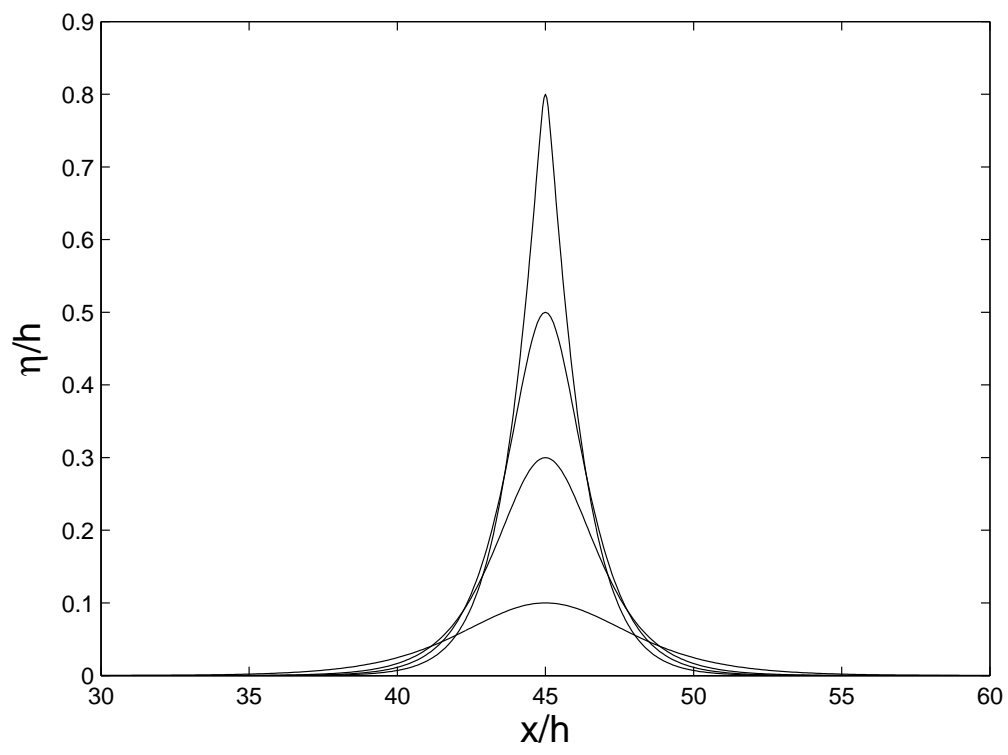


FIG. 1: Solitary waves of height $S/h = 0.1, 0.3, 0.5, 0.8$ computed by the modified Tanaka's method.

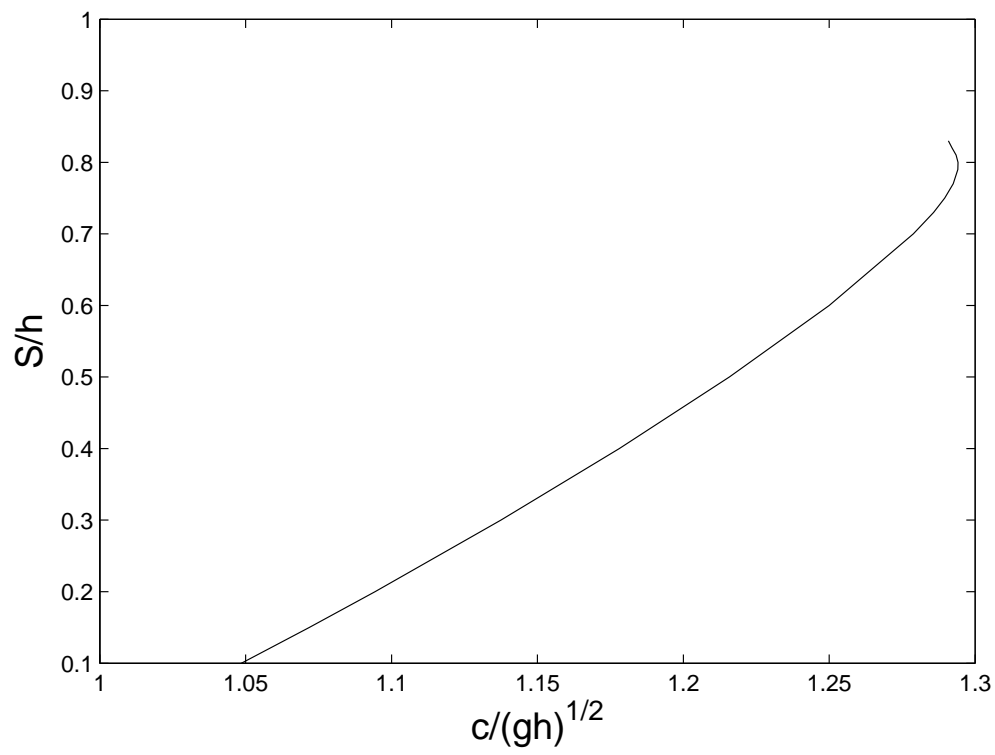


FIG. 2: Bifurcation branch amplitude vs. speed for solitary waves of the Euler equations, computed by the modified Tanaka's method.

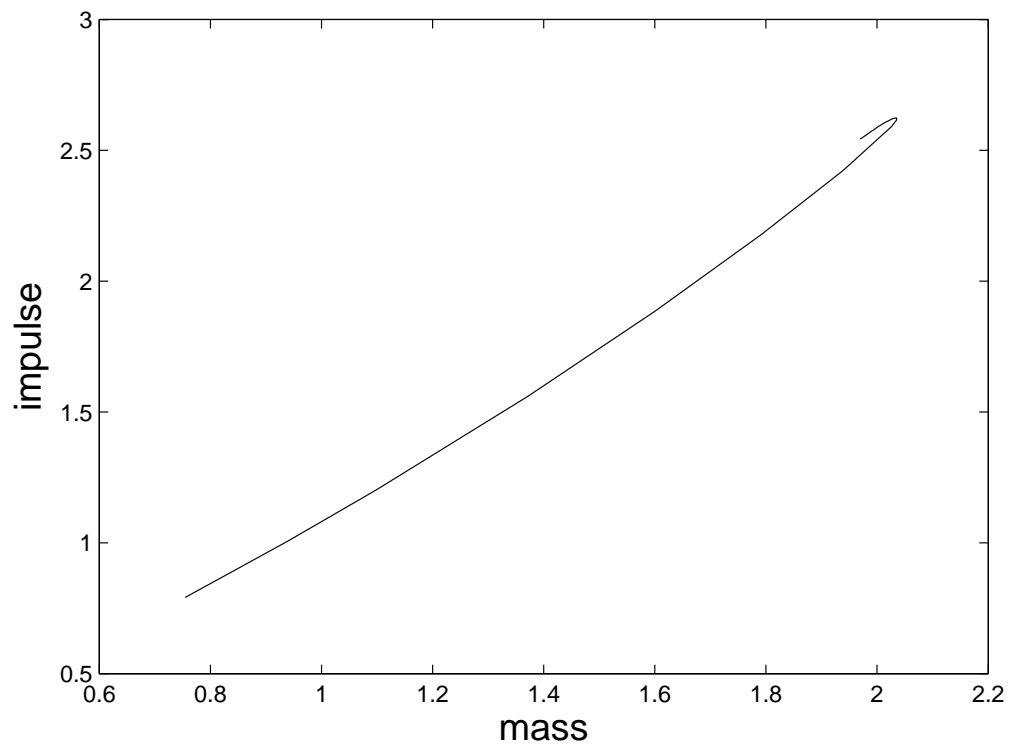
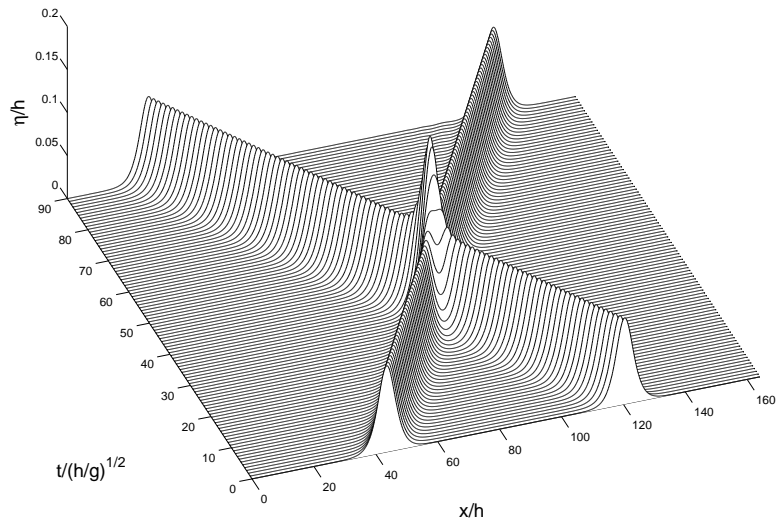


FIG. 3: Impulse vs. mass for solitary waves of the Euler equations of amplitudes $S/h = 0.1$ to 0.8 , computed by the modified Tanaka's method. Note the convexity of the graph over the range $0.8 \leq m \leq 1.9$.

(a)



(b)

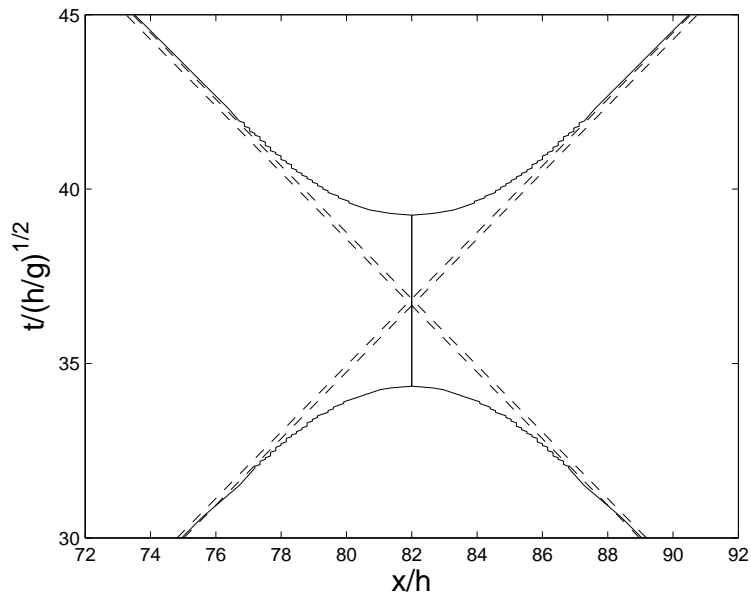
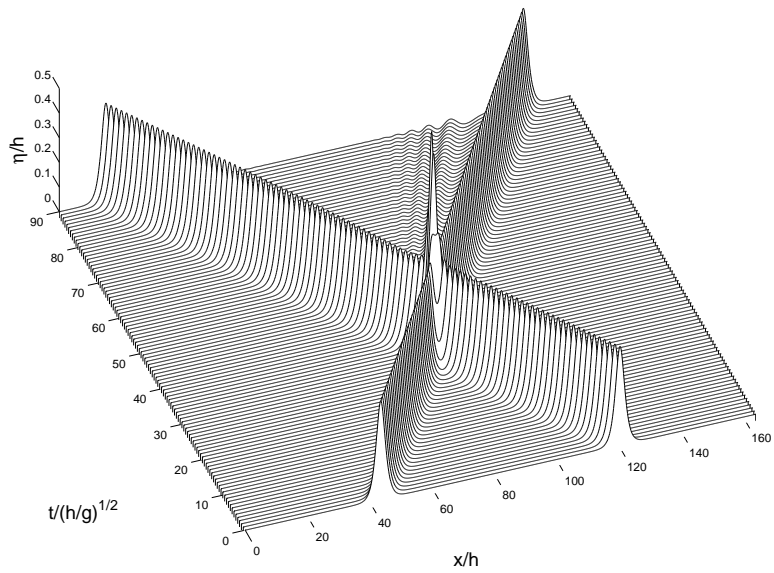


FIG. 4: Head-on collision of two solitary waves of equal height $S/h = 0.1$: (a) (x, t) -plot and (b) crest trajectory. The amplitude after collision is $S^+/h = 0.0997$ at $t/\sqrt{h/g} = 90$. The phase lag is $(a_j - a_j^+)/h = 0.1370$.

(a)



(b)

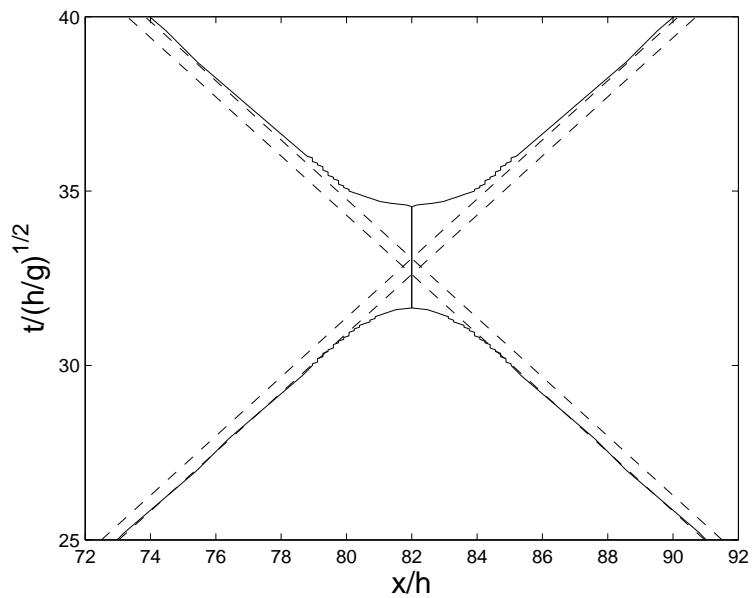


FIG. 5: Head-on collision of two solitary waves of equal height $S/h = 0.4$: (a) (x, t) -plot and (b) crest trajectory. The amplitude after collision is $S^+/h = 0.3976$ at $t/\sqrt{h/g} = 90$. The phase lag is $(a_j - a_j^+)/h = 0.3257$.

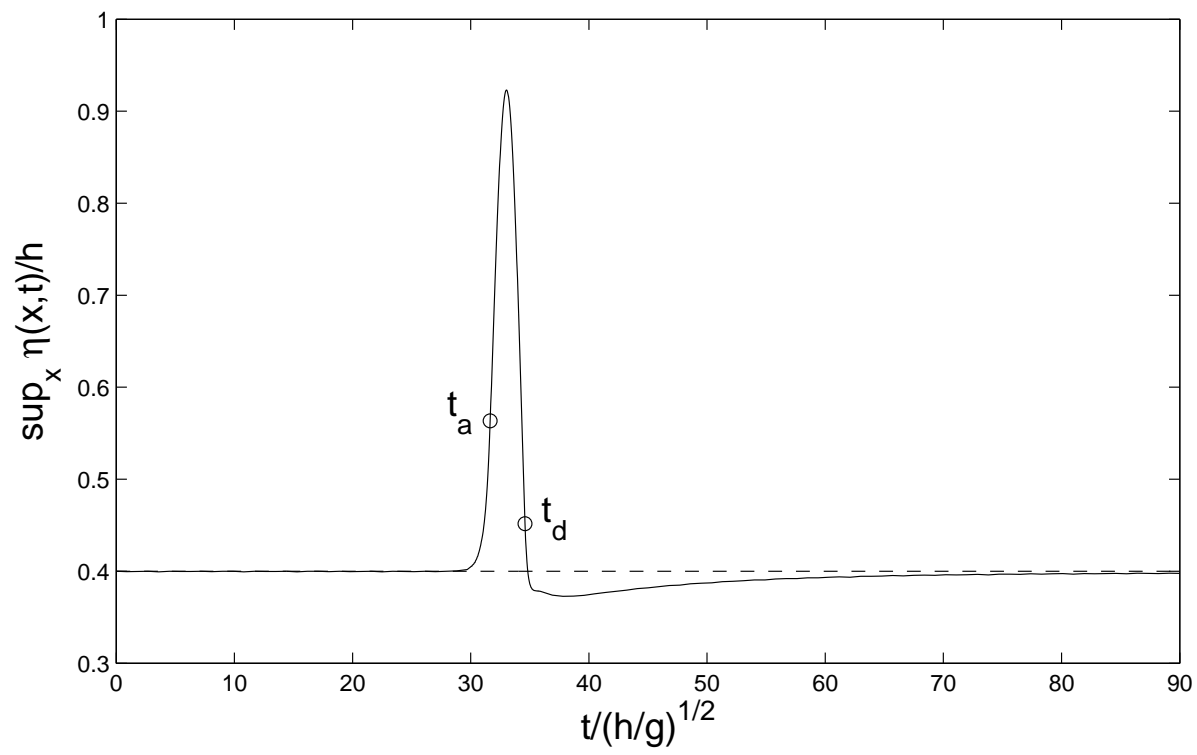


FIG. 6: Time evolution of the amplitude $\|\eta(x, t)\|_{L^\infty(\mathbb{R}_x)}$ for the head-on collision of two solitary waves of equal height $S/h = 0.4$. The attachment and detachment times t_a and t_d are represented by circles. This is comparable to Figs. 4(a)(b) of Cooker, Weidman and Bale [4].

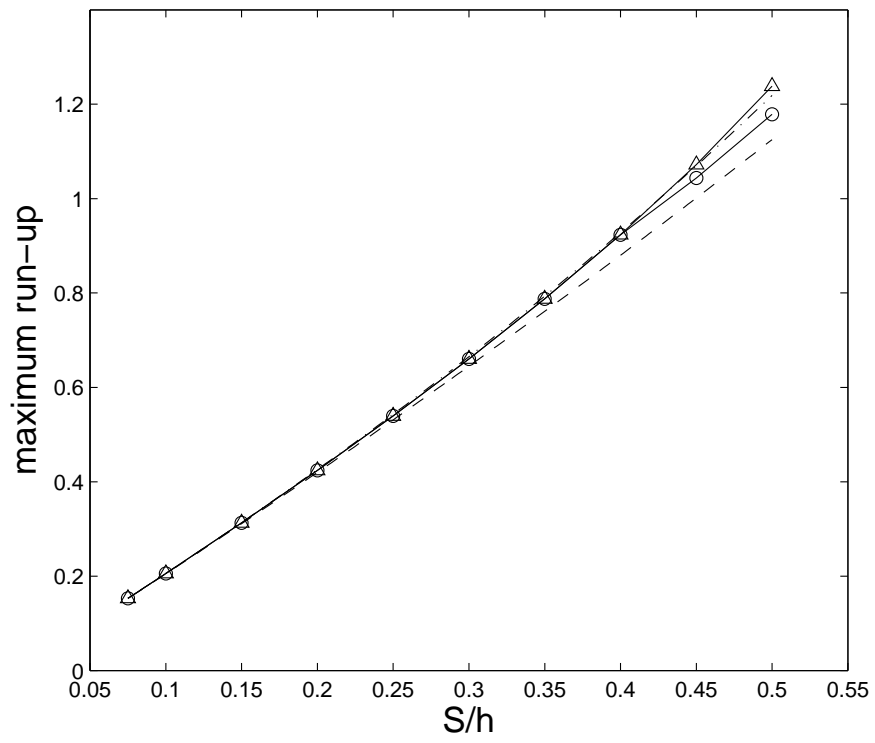


FIG. 7: Maximum run-up as a function of incident wave height: our numerical results (solid line-circles), numerical results of Cooker, Weidman and Bale [4] (solid line-triangles), perturbation results to second-order (dashed line) and third-order (dotted-dashed line) reported in Su and Mirie [6].

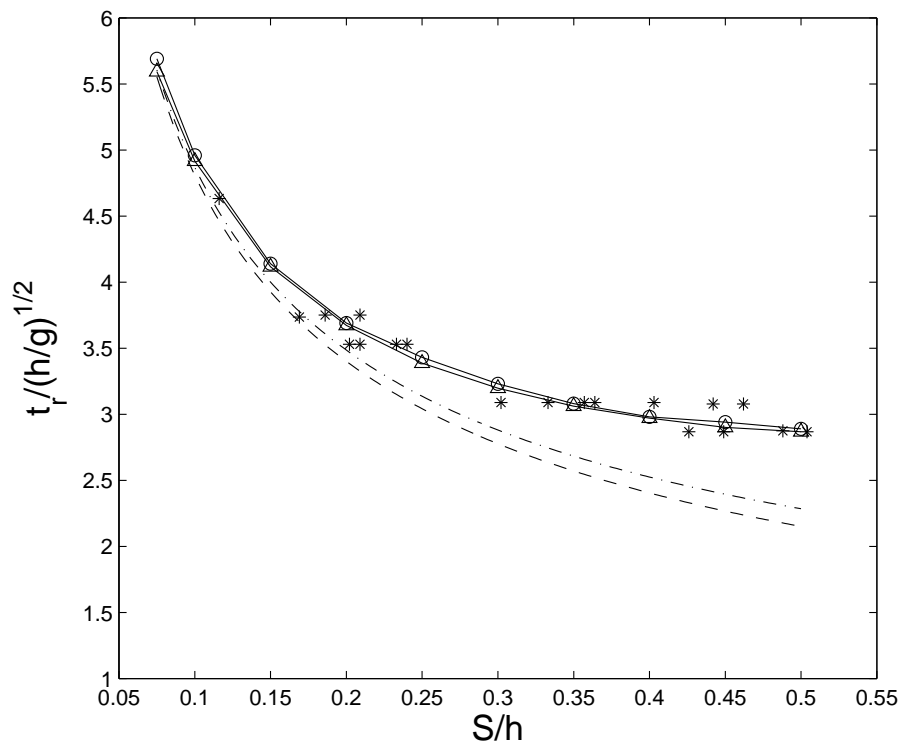
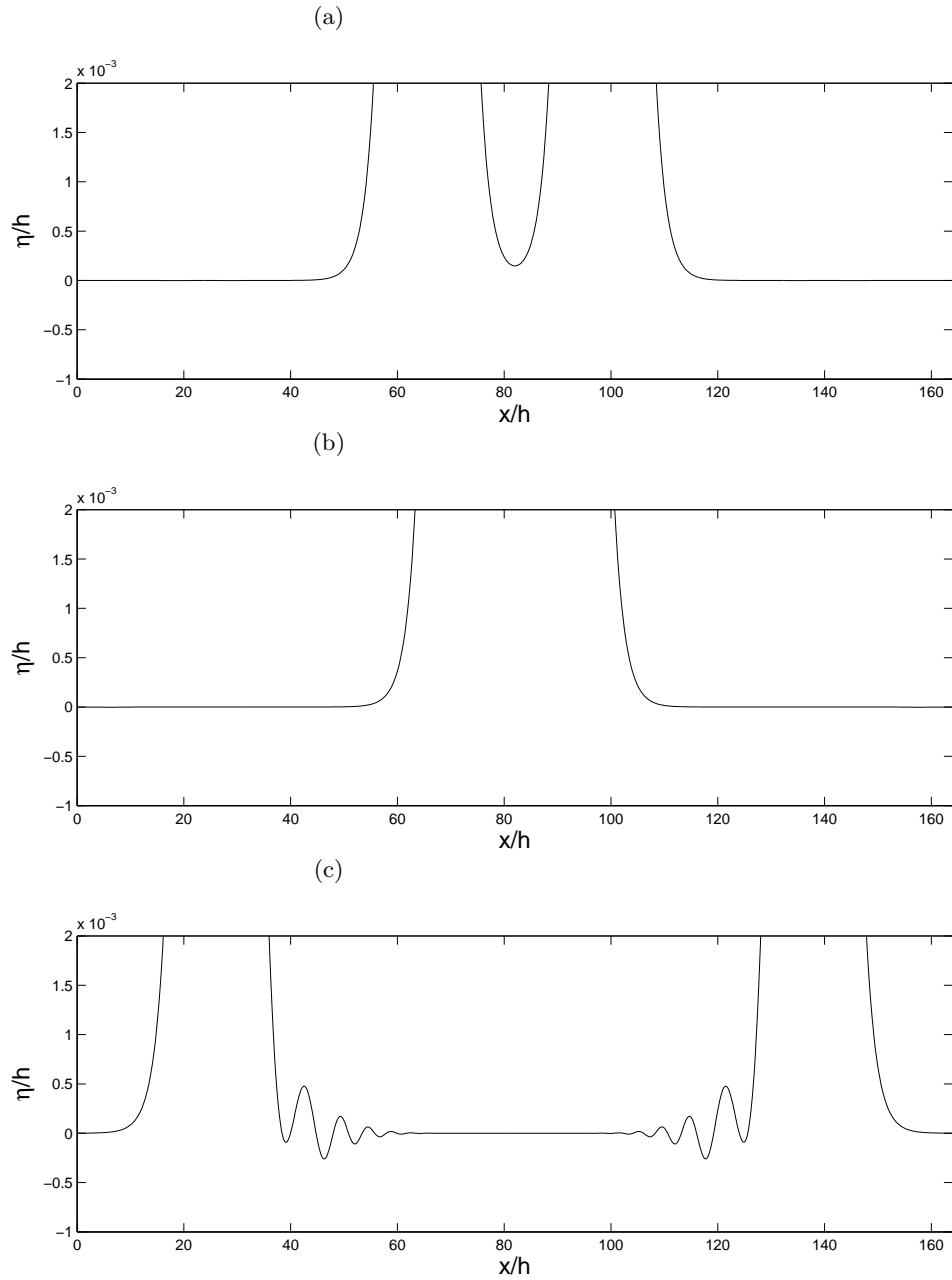


FIG. 8: Wall residence time as a function of incident wave height: our numerical results (solid line-circles), numerical results of Cooker, Weidman and Bale [4] (solid line-triangles), experimental results of Maxworthy [5] (stars), perturbation results to second-order (dashed line) and third-order (dotted-dashed line) following Su and Mirie [6].



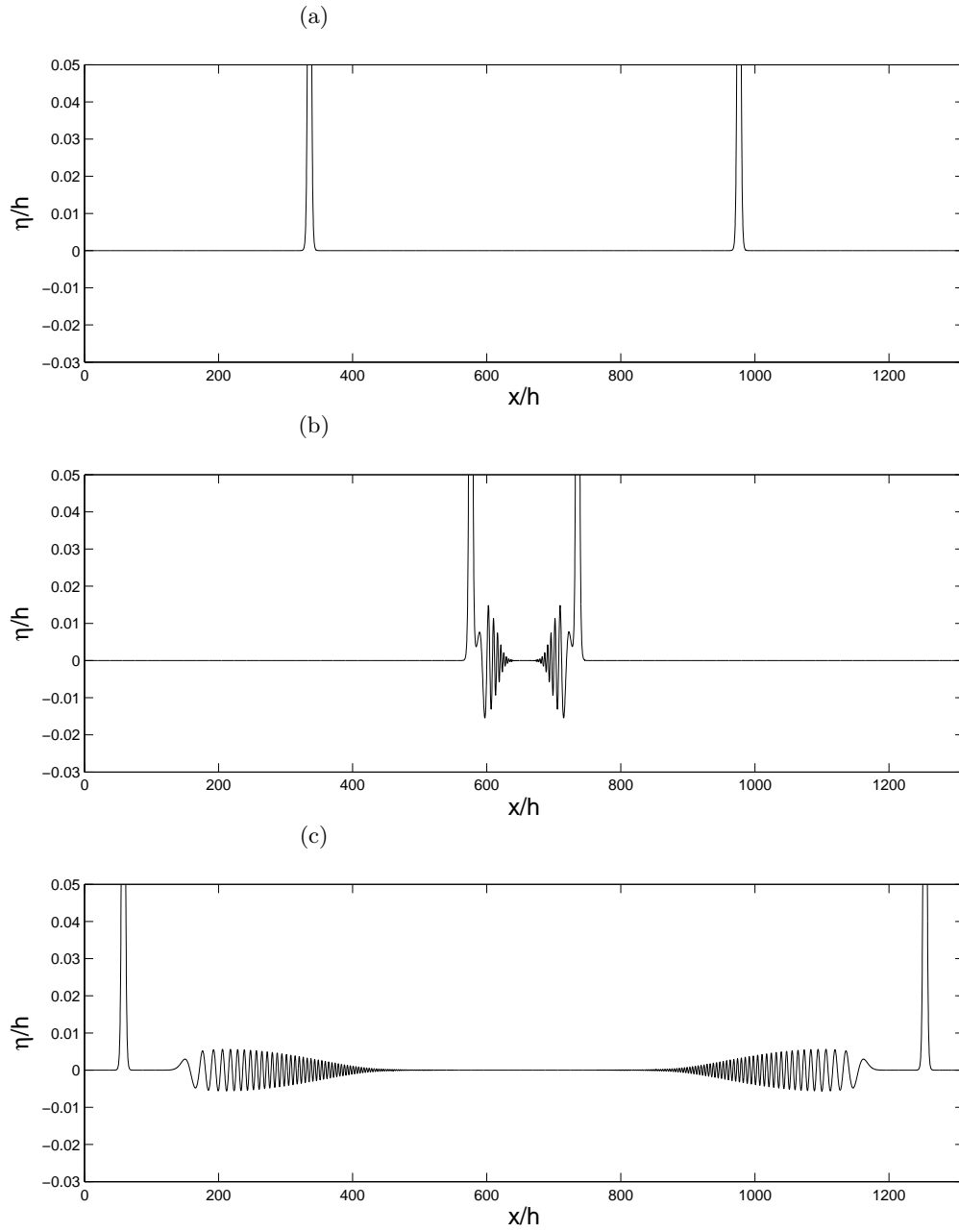


FIG. 10: Head-on collision of two solitary waves of equal height $S/h = 0.4$ which are initially well separated from each other, at (a) $t/\sqrt{h/g} = 0$, (b) 340, (c) 780.

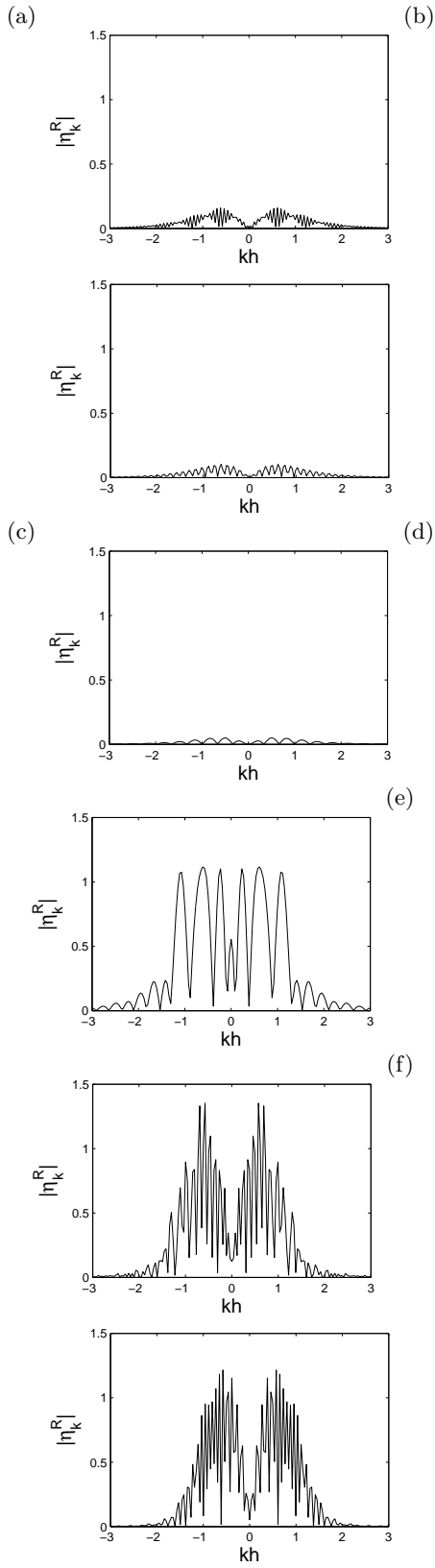


FIG. 11: Fourier spectrum of the residual η_R at (a) $t/\sqrt{h/g} = 0.02$, (b) 13.20, (c) 24.60, (d) 42.90, (e) 66.00, (f) 89.10, for the head-on collision of two solitary waves of equal height $S/h = 0.4$. For comparison, the Fourier spectrum of the solitary wave component of the full solution $\eta_S(x)$ is of amplitude 19.9870.

S/h	S^+/h	$(S - S^+)/h$	E_T	$e_R (\times 10^3)$	$\frac{e_R}{E_T} (\times 10^3)$
0.025	0.02490	0.00010	0.011	0.092	8.358
0.05	0.04983	0.00017	0.034	0.192	5.564
0.075	0.07476	0.00024	0.065	0.338	5.174
0.1	0.09964	0.00036	0.102	0.598	5.865
0.15	0.14930	0.00070	0.191	1.378	7.203
0.2	0.19892	0.00108	0.299	2.517	8.403
0.25	0.24859	0.00141	0.425	3.809	8.968
0.3	0.29834	0.00166	0.565	5.400	9.562
0.35	0.34788	0.00212	0.718	7.791	10.855
0.4	0.39738	0.00262	0.882	8.817	9.999
0.45	0.44534	0.00466	1.054	16.323	15.488
0.5	0.49311	0.00689	1.231	24.712	20.067

TABLE I: Ratio of the amplitude loss, and comparison of the energy of the residual with the total energy at $t/\sqrt{h/g} = 80$ as a function of incident wave height, for the head-on collision of two solitary waves of equal height.

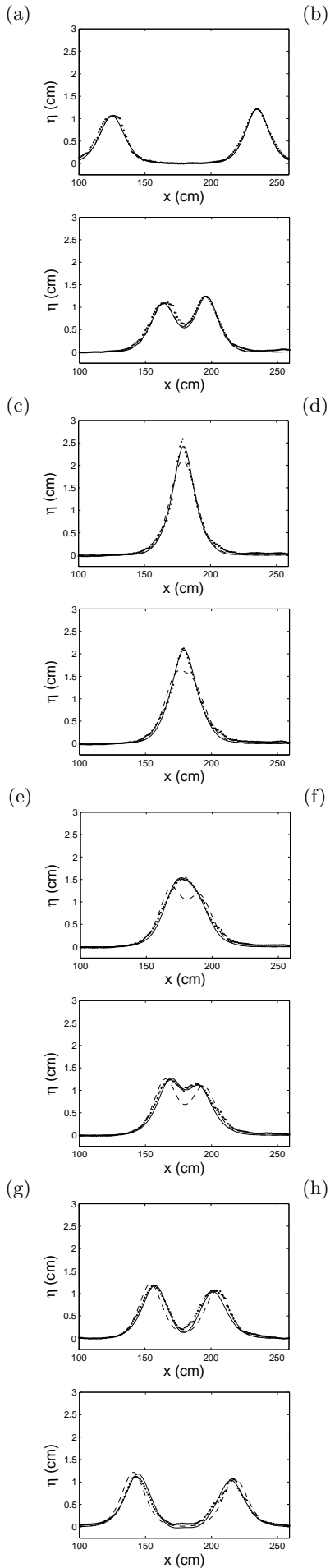
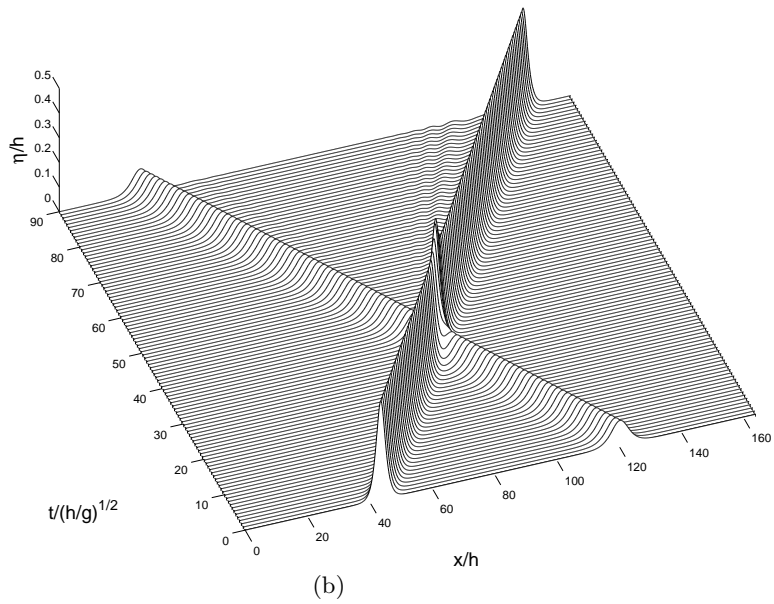


FIG. 12: Asymmetric head-on collision of two solitary waves of height $S_1 = 1.217$, $S_2 = 1.063$ (cm) at (a) $t = 18.29993$, (b) 18.80067, (c) 19.05257, (d) 19.10173, (e) 19.15088, (f) 19.19389, (g) 19.32905, (h) 19.50109 (s): numerical results (solid line), experimental results (dots), sum of two KdV solitons (dashed line).

(a)



(b)

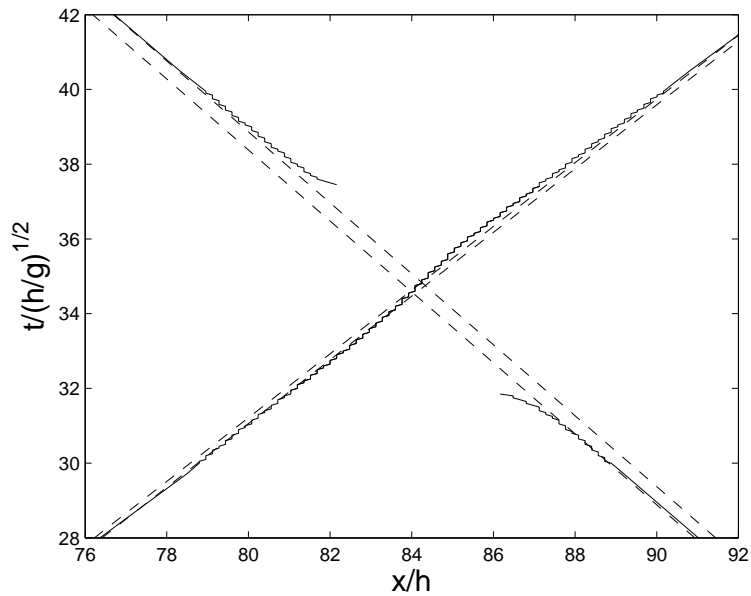
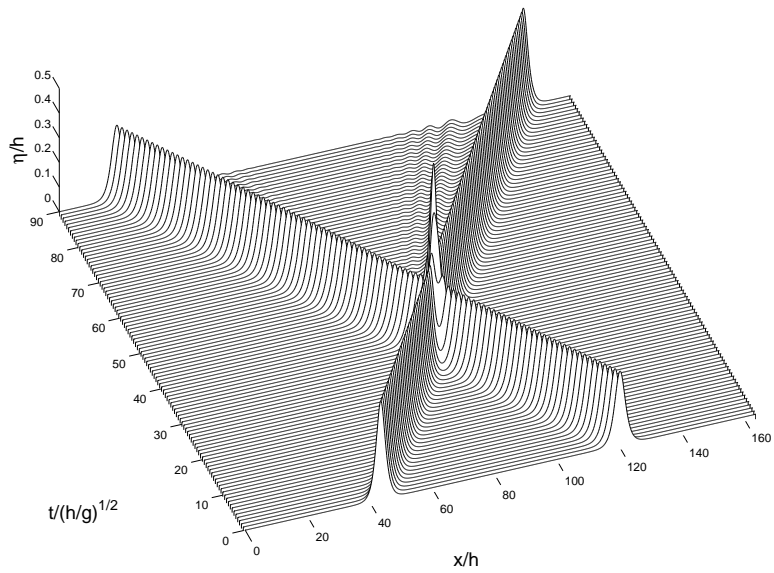


FIG. 13: Asymmetric head-on collision of two solitary waves of height $S_1/h = 0.4$, $S_2/h = 0.1$: (a) (x, t) -plot and (b) crest trajectory. The amplitudes after collision are $S_1^+/h = 0.3996$, $S_2^+/h = 0.0992$ at $t/\sqrt{h/g} = 90$ for the large, small wave respectively. The phase lags are $(a_1 - a_1^+)/h = 0.1211$, $(a_2 - a_2^+)/h = 0.3597$ respectively.

(a)



(b)

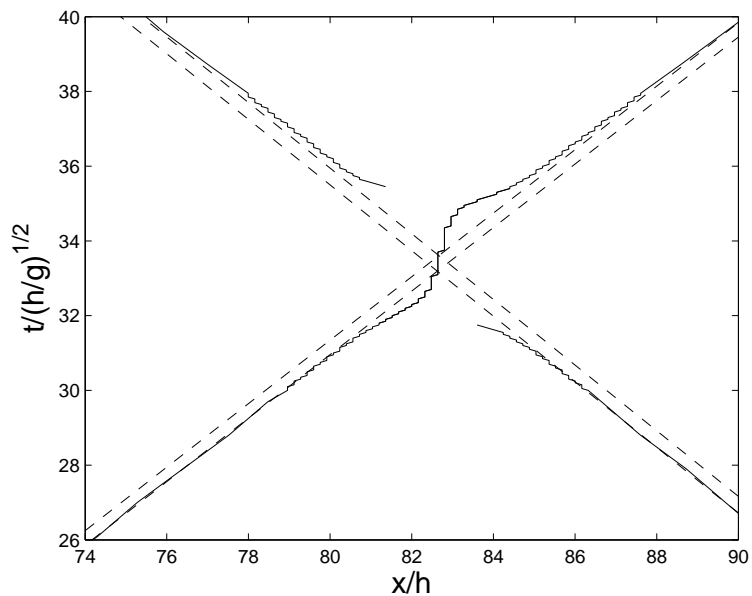


FIG. 14: Asymmetric head-on collision of two solitary waves of height $S_1/h = 0.4$, $S_2/h = 0.3$: (a) (x, t) -plot and (b) crest trajectory. The amplitudes after collision are $S_1^+/h = 0.3987$, $S_2^+/h = 0.2983$ at $t/\sqrt{h/g} = 90$ for the large, small wave respectively. The phase lags are $(a_1 - a_1^+)/h = 0.3021$, $(a_2 - a_2^+)/h = 0.3223$ respectively.

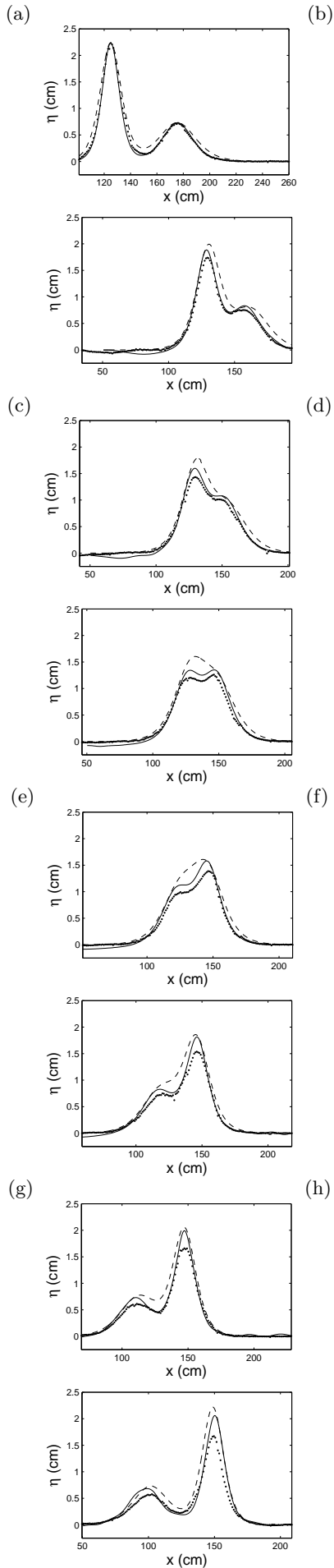
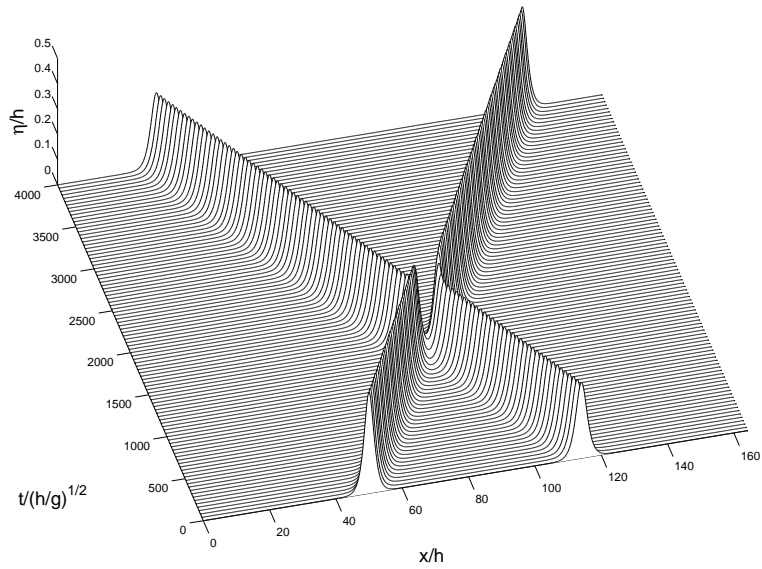


FIG. 15: Overtaking collision of two solitary waves of heights $S_1 = 2.295$, $S_2 = 0.730$ (cm) at (a) $t = 2.90304$, (b) 5.50196 , (c) 6.40513 , (d) 7.05025 , (e) 7.60014 , (f) 8.50024 , (g) 9.50478 , (h) 11.30191 (s): numerical results (solid line), experimental results (dots), KdV two-soliton solution (dashed line). The three sets of data are plotted in a reference frame with zero

(a)



(b)

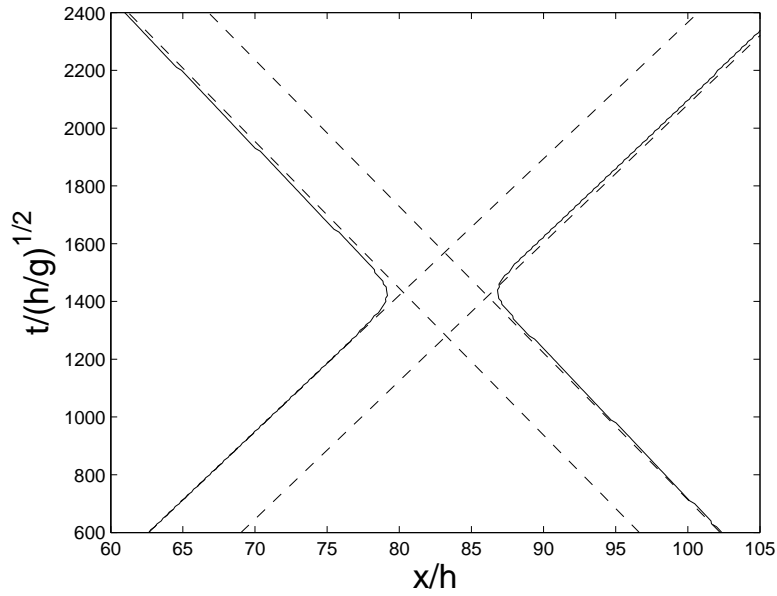
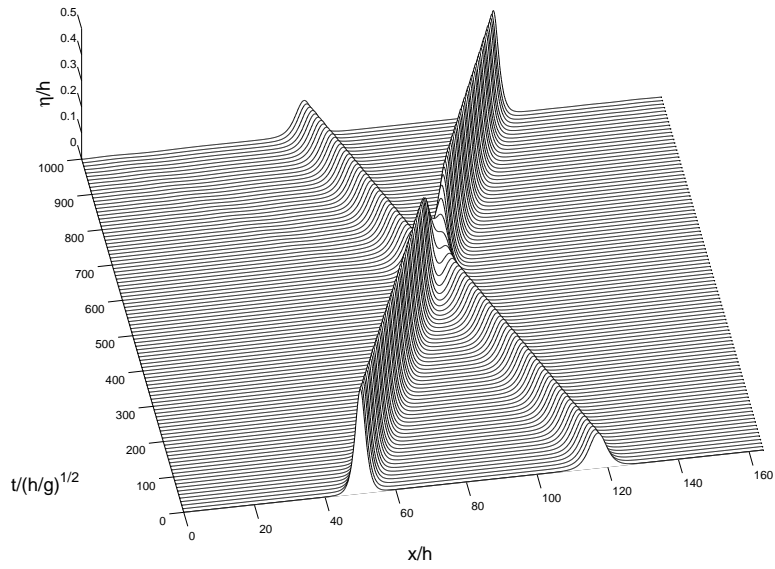


FIG. 16: Overtaking collision of two solitary waves of height $S_1/h = 0.4$, $S_2/h = 0.3$: (a) (x, t) -plot and (b) crest trajectory. The amplitudes after collision are $S_1^+/h = 0.4004$, $S_2^+/h = 0.2999$ at $t/\sqrt{h/g} = 4000$ for the large, small wave respectively. The phase shifts are $(a_1^+ - a_1)/h = 6.5665$, $(a_2^+ - a_2)/h = 5.6194$ respectively. The collision is represented in a reference frame moving approximately with the mean velocity of the two solitary waves.

(a)



(b)

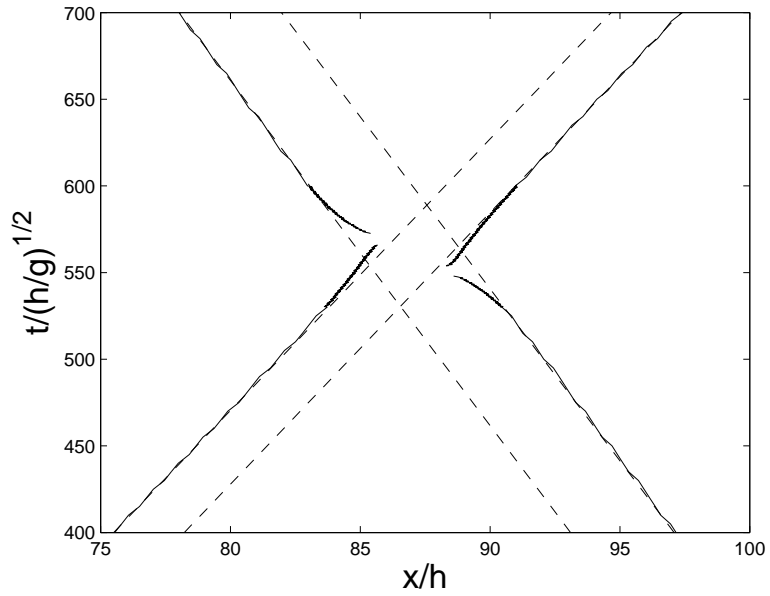
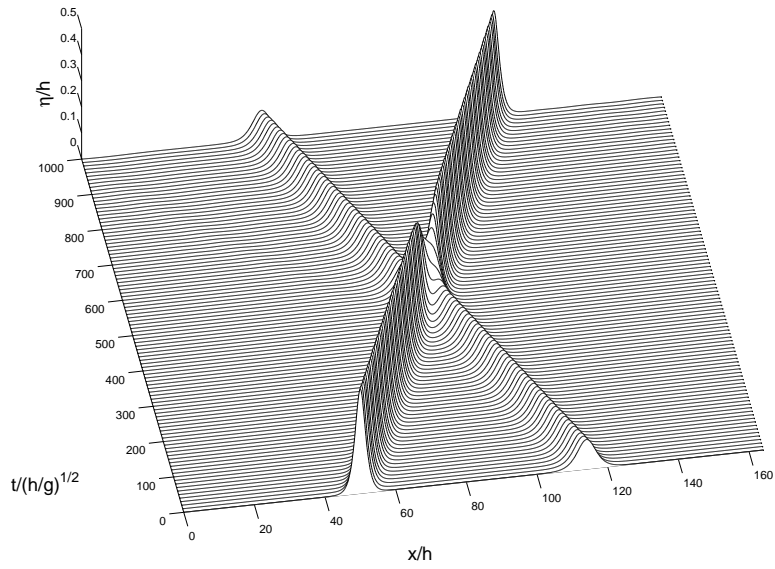


FIG. 17: Overtaking collision of two solitary waves of height $S_1/h = 0.4$, $S_2/h = 0.1333$: (a) (x, t) -plot and (b) crest trajectory. The amplitudes after collision are $S_1^+/h = 0.4001$, $S_2^+/h = 0.1332$ at $t/\sqrt{h/g} = 1000$ for the large, small wave respectively. The phase shifts are $(a_1^+ - a_1)/h = 2.7424$, $(a_2^+ - a_2)/h = 4.0591$ respectively.

(a)



(b)

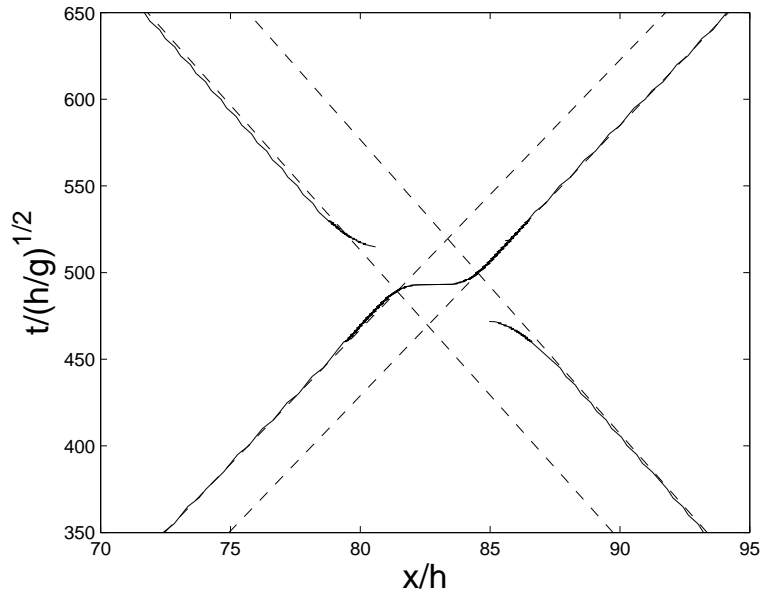
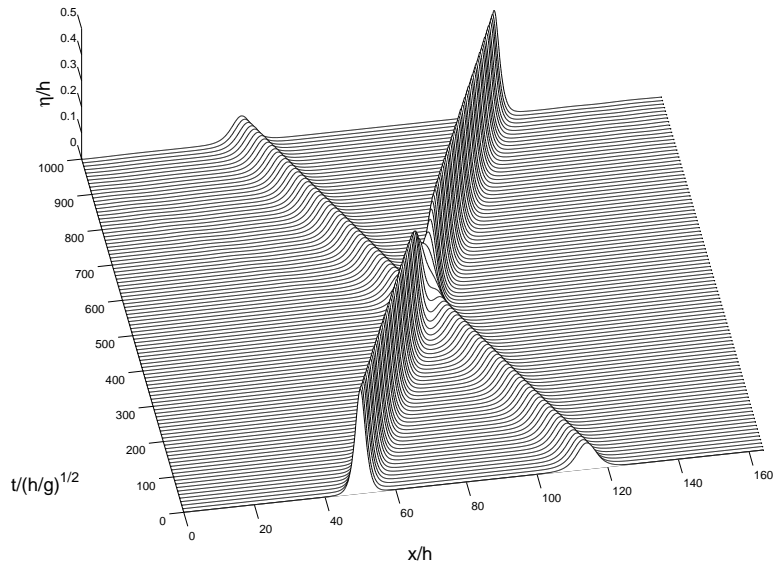


FIG. 18: Overtaking collision of two solitary waves of height $S_1/h = 0.4$, $S_2/h = 0.113$: (a) (x, t) -plot and (b) crest trajectory. The amplitudes after collision are $S_1^+/h = 0.4001$, $S_2^+/h = 0.1129$ at $t/\sqrt{h/g} = 1000$ for the large, small wave respectively. The phase shifts are $(a_1^+ - a_1)/h = 2.5462$, $(a_2^+ - a_2)/h = 3.3274$ respectively.

(a)



(b)

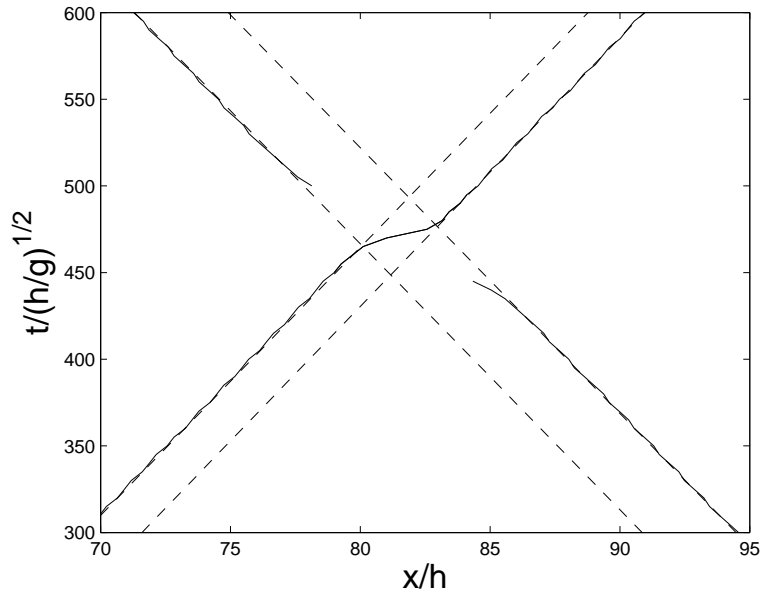


FIG. 19: Overtaking collision of two solitary waves of height $S_1/h = 0.4$, $S_2/h = 0.1$: (a) (x, t) -plot and (b) crest trajectory. The amplitudes after collision are $S_1^+/h = 0.4003$, $S_2^+/h = 0.0999$ at $t/\sqrt{h/g} = 1000$ for the large, small wave respectively. The phase shifts are $(a_1^+ - a_1)/h = 2.2974$, $(a_2^+ - a_2)/h = 3.6159$ respectively.

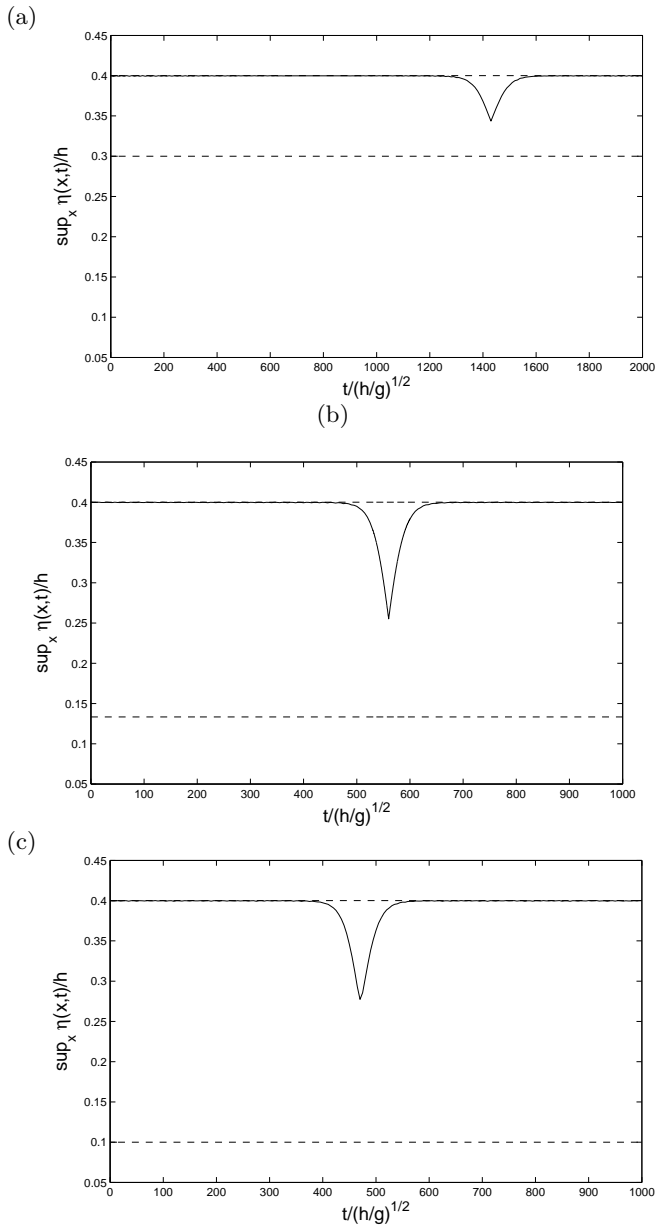
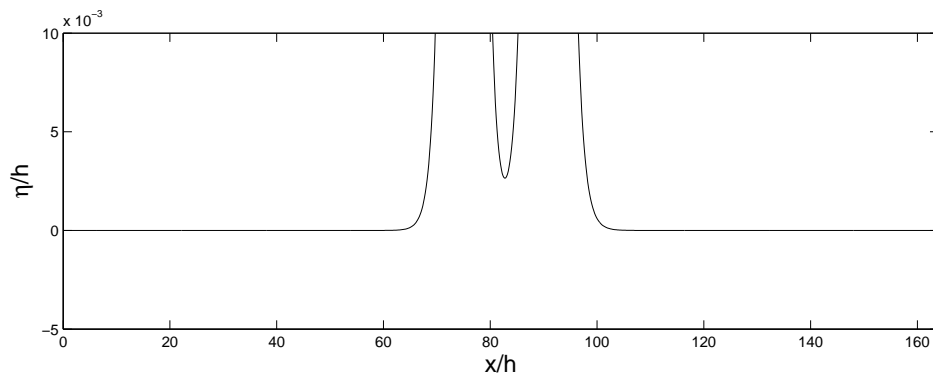
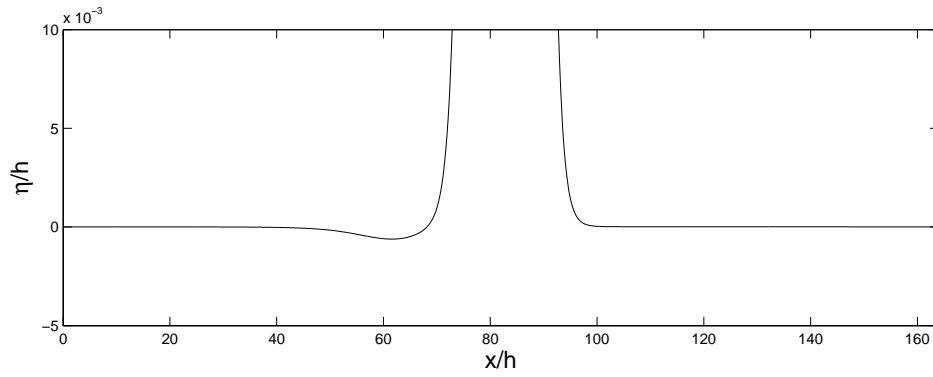


FIG. 20: Time evolution of the amplitude $\|\eta(x, t)\|_{L^\infty(\mathbb{R}_x)}$ for the overtaking collision of two solitary waves of height (a) $S_1/h = 0.4$, $S_2/h = 0.3$, (b) $0.4, 0.1333$ and (c) $0.4, 0.1$.

(a)



(b)



(c)

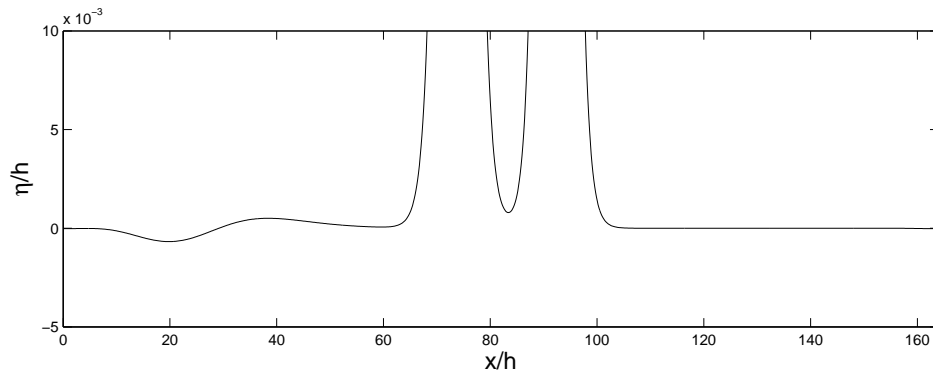


FIG. 21: Overtaking collision of two solitary waves of height $S_1/h = 0.4$, $S_2/h = 0.3$ at (a) $t/\sqrt{h/g} = 1190$ (before collision), (b) 1490 (during collision), (c) 1740 (after collision). The vertical scale is magnified in order to observe the dispersive trailing wave generated after the collision.

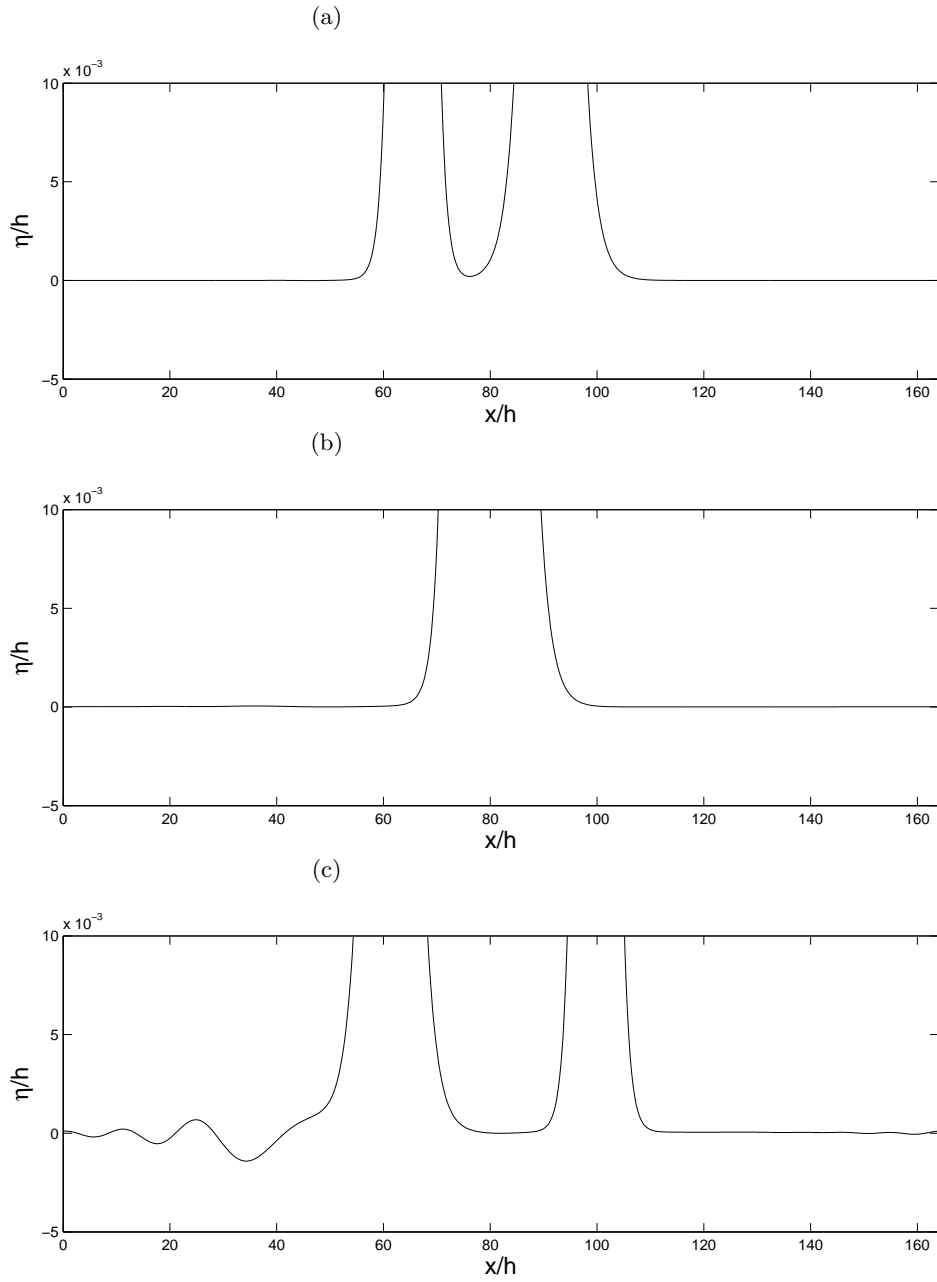


FIG. 22: Overtaking collision of two solitary waves of height $S_1/h = 0.4$, $S_2/h = 0.1$ at (a) $t/\sqrt{h/g} = 295$ (before collision), (b) 445 (during collision), (c) 745 (after collision). The vertical scale is magnified in order to observe the dispersive trailing wave generated after the collision.

S_1/h	S_1^+/h	$(S_1^+ - S_1)/h$	S_2/h	S_2^+/h	$(S_2 - S_2^+)/h$	E_T	e_R	$\frac{e_R}{E_T}$	Category
							($\times 10^5$)	($\times 10^5$)	
0.4	0.4004	0.0004	0.3	0.2999	0.0001	0.689	19.458	28.235	(a)
0.4	0.4001	0.0001	0.1333	0.1332	0.0001	0.497	8.310	16.717	(b)
0.4	0.4001	0.0001	0.113	0.1129	0.0001	0.480	7.801	16.235	(c)
0.4	0.4003	0.0003	0.1	0.0999	0.0001	0.471	1.886	4.001	(c)

TABLE II: Ratio of the amplitude loss, and comparison of the energy e_R of the residual to the total energy E_T of the full numerical solution at $t/\sqrt{h/g} = 4000$ ($S_2/h = 0.3$), $t/\sqrt{h/g} = 1000$ ($S_2/h = 0.1333, 0.113, 0.1$) as a function of incident wave heights, for the overtaking collision of two solitary waves of different heights.

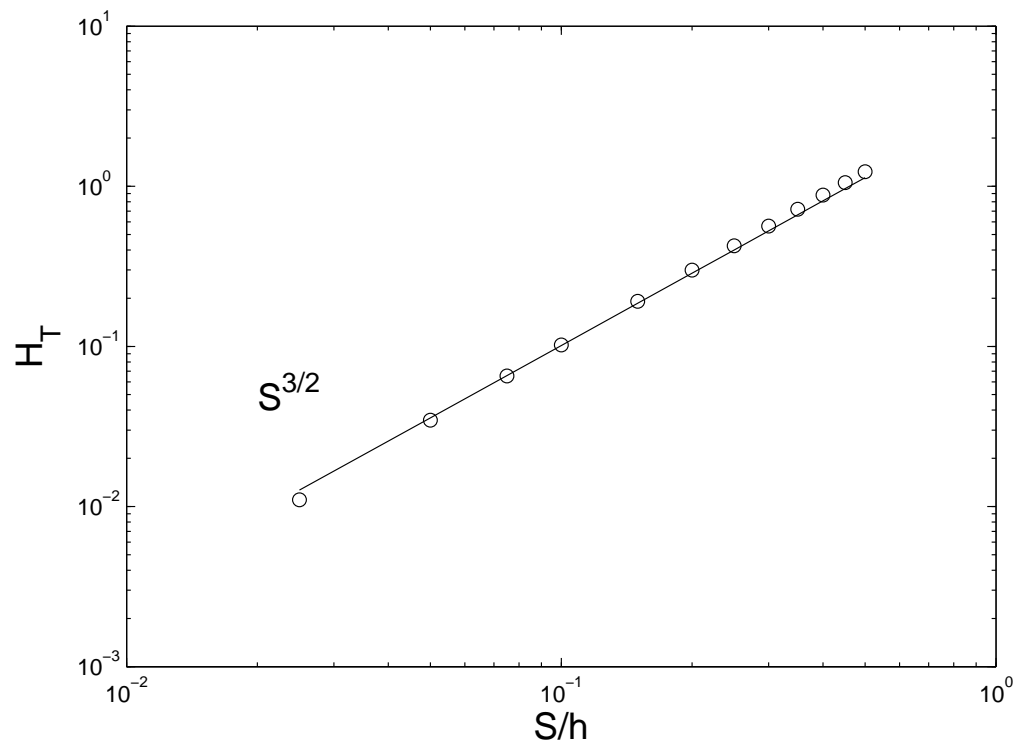


FIG. 23: Total energy E_T vs. wave amplitude S/h : numerical results (circles), power law $(S/h)^{3/2}$ (solid line).

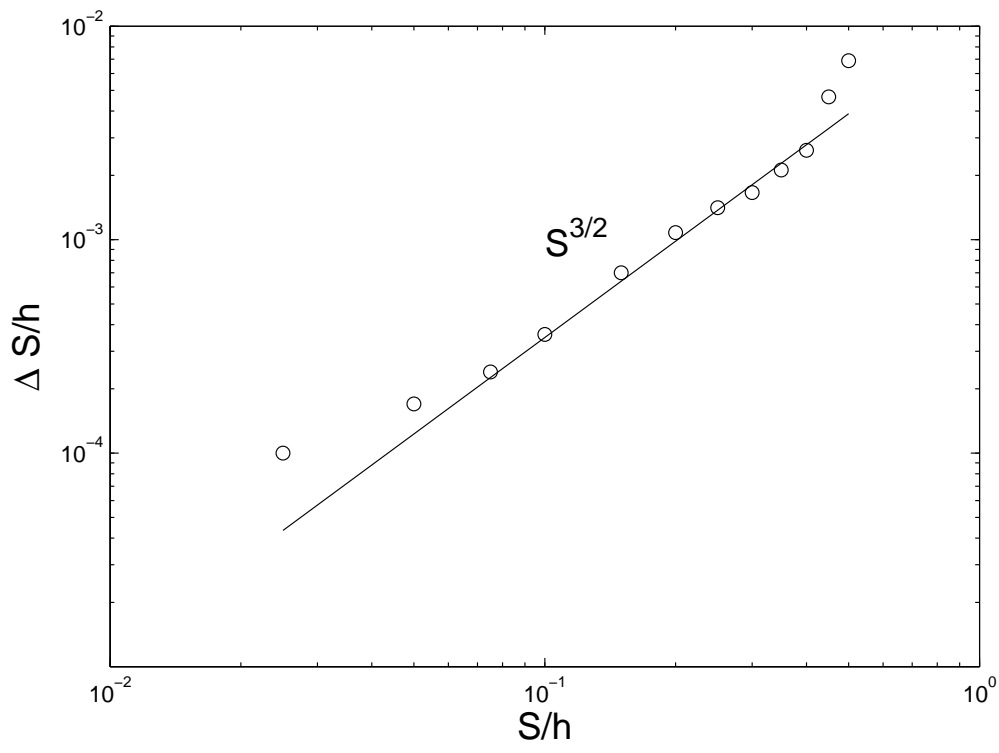


FIG. 24: Change in amplitude $\Delta S/h = (S - S^+)/h$ vs. wave amplitude S/h : numerical results (circles), power law $(S/h)^{3/2}$ (solid line).

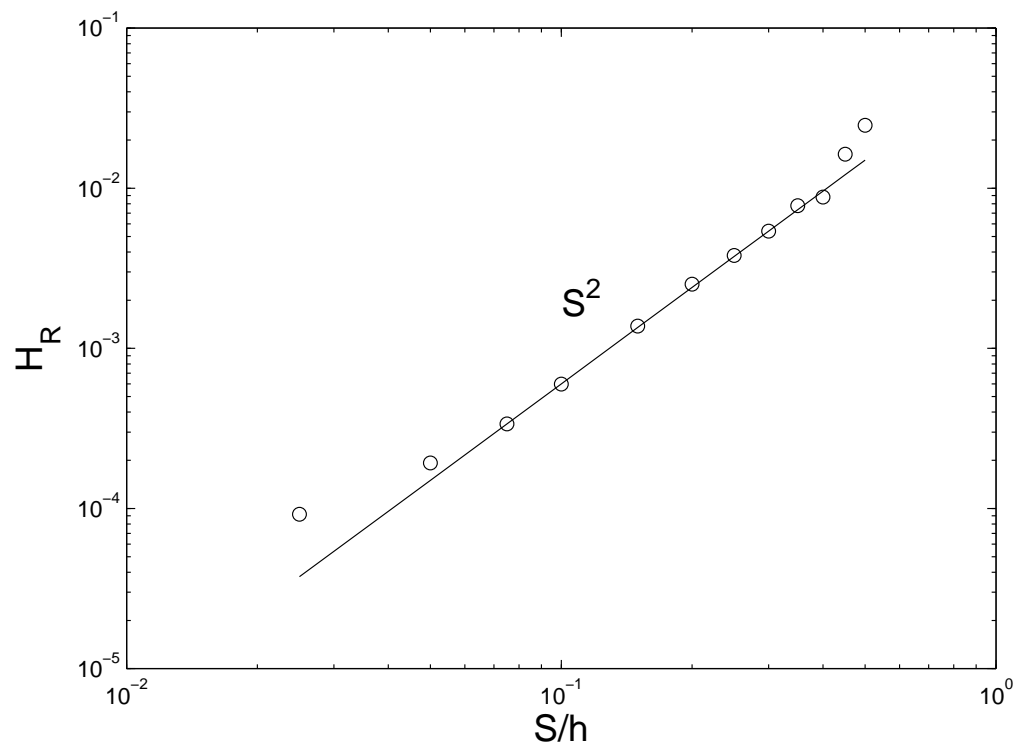


FIG. 25: Energy of the residual e_R vs. nondimensional wave amplitude S/h : numerical results (circles), power law $(S/h)^2$ (solid line).